Universidade de Aveiro Departamento de Ciências Médicas
Ano 2018

ANA ANDREIA MENDES TEIXEIRA

Estudo do metabolismo do NAD na agregação proteica

Study of NAD metabolism in protein aggregation

Universidade de Aveiro Departamento de Ciências Médicas
Ano 2018

ANA ANDREIA MENDES TEIXEIRA

Estudo do metabolismo do NAD na agregação proteica

Study of NAD metabolism in protein aggregation

Tese apresentada à Universidade de Aveiro para cumprimento dos requisitos necessários à obtenção do grau de Mestre em Biomedicina Molecular, realizada sob a orientação científica da Doutora Raquel M Silva, Professora Auxiliar Convidada do Departamento de Ciências Médicas da Universidade de Aveiro.

This work was supported by FEDER (Programa Operacional Factores de Competitividade – COMPETE) and by FCT (Fundação para a Ciência e Tecnologia), within the project UID/BIM/04501/2013 and POCI-01-0145-FEDER-007628 to iBiMED, and by the Integrated Programme of SR&TD “pAGE - Protein aggregation across the lifespan” (reference CENTRO-01-0145-FEDER-000003), co-funded by Centro 2020 program, Portugal 2020, European Union, through the European Regional Development Fund.

o júri

presidente

Prof. Doutor Ramiro Almeida
professor auxiliar do Departamento de Ciências Médicas da Universidade de Aveiro

Prof. Doutora Raquel M Silva
professora auxiliar convidada do Departamento de Ciências Médicas da Universidade de Aveiro

Prof. Doutora Antje Garten
investigadora do Center for Pediatric Research da Universidade de Leipzig

agradecimentos

The present study is the combination of hard work and the contribution of many people, to whom I want to express my sincere gratitude.

My first thank you goes to **Aveiro University**, specially to the Medical Sciences Department for accepting me in the Master programme and all knowledge I acquired here and to the **Institute of Biomedicine**, iBiMED, where this work was developed. To **Dra. Catarina Almeida** for the help with the cytometry and to **Mariana Alves** from the LiM facility of iBiMED (a node of PPBI - Portuguese Platform of BioImaging: POCI-01-0145-FEDER-022122) and **Isabel Pereira-Castro** from the i3S for the help with the confocal microscopy.

A special thank you to **Dra. Raquel Silva** for all the things that I have learned from you, for all the effort and commitment with this study and for all the hours you have spent teaching me. Thank you for helping me during the last year and for all ideas and discussion. Thank you for the opportunities that you propose to me. I really loved working with you and in the future, I hope to pass my knowledge the same way you do. You will always be an example for me.

To **Diogo Neves**, for so many hours you have spent with me, for the effort you put in this project, for all the kindness and for all emotional conversations. You were and are a great mentor.

To **NAD group**, for all funny meetings and for all ideas discussed. I loved work with you.

To **Sónia, Tânia,** and **Guida**, that were always there for me, even at long distance. Thank you for all the support during all my life, mainly in the biggest and important moments.

To **Beatriz** and **Flávia**, that were always there for me in the last two years. Thank you for all the support, for having deal with my bad mood so many times and for never let me dishearten.

To **Lara**, the best home-partner ever. Thank you for being my emotional support in the last two years. You´re the best and certainly, we gonna live in a wonderful world for ever.

To **Hélder**, a big thank you for all support, for all interest about this work. Thank you for listening me so many times and thank you for all love.

The last and the biggest thank you goes to my **mother** and **father**, the inspiration of my dreams and for teaching me that no luck comes without hard work. Thank you for always believing in me and in my dreams and for being proud of me in every step of my life. I love you so much.

palavras-chave

Biosíntese de NAD, NAD, NAMPT, NAPRT, NMNAT-2, Precursores de NAD, Agregação proteica, Viabilidade celular, Estado metabólico, Expressão génica, Envelhecimento

resumo

NAD (Nicotinamida Adenina Dinucleótido) é uma piridina envolvida em vários processos biológicos, nomeadamente, catabolismo de nutrientes que sustentam a produção de energia na célula. Durante o envelhecimento, os níveis de NAD diminuem e uma desregulação global da proteostase é observada. Como muitas doenças ligadas ao envelhecimento são neurodegenerativas, onde ocorre acumulação de agregados de proteínas, colocamos a hipótese que o NAD poderá prevenir ou melhorar a agregação proteica. Para estudar o papel do metabolismo do NAD na proteostase, expusemos células SH-SY5Y a químicos que modelam os níveis de agregação proteica e de NAD. As células foram marcadas com o kit ProteoStat® para detetar os agregados proteicos e analisadas por citometria de fluxo e microscopia confocal. A viabilidade celular foi medida com iodeto de propídio por citometria de fluxo e o estado metabólico foi medido usando o ensaio colorimétrico da resazurina. Células SH-SY5Y apresentaram um aumento de agregados proteicos na presença do inibidor de proteossoma MG132 ao longo do tempo. MG132 induziu mais agregação do que o tratamento com um inibidor do metabolismo de NAD, no entanto a suplementação com NAD pareceu diminuir esses agregados. A microscopia confocal corroborou os resultados de citometria de fluxo. Em todas as condições testadas, a viabilidade celular não foi alterada, em contraste com o estado metabólico que foi alterado pelos tratamentos. Suplementação com NAD pareceu diminuir a agregação proteica e estudos futuros serão necessários para elucidar o papel na proteostase dos diferentes precursores de NAD e vias metabólicas associadas.

keywords

NAD biosynthesis, NAD, NAMPT, NAPRT, NMNAT-2, NAD precursors, Protein aggregation, Cell viability, Metabolic state, Gene expression, Aging

abstract

NAD (Nicotinamide Adenine Dinucleotide) is a pyridine involved in numerous biological processes, namely nutrient catabolism sustaining cellular energy metabolism. During aging, NAD levels decrease and a global proteostasis deregulation is observed. As many age-related diseases are neurodegenerative and characterized by the accumulation of protein aggregates, we hypothesized that NAD could prevent or ameliorate protein aggregation. To study the role of NAD metabolism in proteostasis, we used SH-SY5Y cells exposed to chemicals that modulate the levels of protein aggregation and NAD metabolism. Cells were stained with the ProteoStat® kit to detect protein aggregates and analysed by flow cytometry and fluorescence microscopy. Cell viability was measured with propidium iodide by flow cytometry and metabolic state was measured using the colorimetric resazurin assay. SH-SY5Y cells showed increased protein aggregation levels in the presence of the proteasome inhibitor MG132 over time. MG132 induced more aggregation than treatment of cells with a NAD metabolism inhibitor, although supplementation with NAD appeared to decrease protein aggregates. Fluorescence microscopy analysis corroborated the flow cytometry result. In all tested conditions cell viability was not altered, in contrast with metabolic state that was altered by chemical treatments. Supplementation with NAD appeared to decrease protein aggregates, and further studies are warranted to elucidate the role in proteostasis of the different NAD precursors and associated pathways.

OUTLINE

LIST OF FIGURES

List of Abbreviations

AA's - Antibiotic-Antimycotic

ACMS - 2-amino-3-carboxymuconic-6-semialdehyde

ADPR - ADP - ribose

AMP - Adenosine Monophosphatase

ANA - Anthranilic Acid

APS - Ammonium Persulfate

ART - ADP-Ribosyltransferase

ATF6 - Activation-transcription Factor 6

ATP - Adenosine Triphosphate

A.U. - Arbitrary Units

BCA - Bovine Serum Albumin

BMAL1 - Aryl Hydrocarbon Receptor Translocated-Like Protein 1

BP - Base pairs

BSA - Bovine Serum Albumin

cADPR - Cyclic ADP-ribose

cDNA - Complementary DNA

CLOCK - Circadian Locomotor Output Cycles Protein Kaput

CR - Calorie Restriction

CsA - Cyclosporin-A

DBC1 - Deleted in Breast Cancer 1

DMSO - Dimethyl sulfoxide

eIF2α - Eukaryotic Translation Initiation Factor 2 Subunit 1

EMT - Epithelial-Mesenchymal Transition

eNAMPT - Extracellular NAMPT

ER - Endoplasmic Reticulum

ERAD - ER-Associated Degradation

FBS - Fetal Bovine Serum

FOXO - Insulin-forkhead Box Protein O

FSC - Forward Scatter

GCN2 - eIF2α Kinase

GRP78 - Glucose-Regulated Protein 78

HRP - Horseradish Peroxidase

HSN - Hypothalamic Suprachiasmatic Nucleus

HSP - Heat Shock Protein

HSR - Heat Shock Response

IDO - Indoleamine 2,3-Dioxygenase

iNAMPT - intracellular NAMPT

IRE1 - Inositol-requiring enzyme 1

kDa - Kilodalton

MEM - Minimum Essential Medium

MFI - Mean Fluorescence Intensity

mTOR - Rapamycin

NA - Nicotinic Acid

NAAD - Nicotinic Acid Adenine Dinucleotide

NAD - Nicotinamide Adenine Dinucleotide; NAD refers globally to the oxidized (NAD^+) and reduced (NADH) forms.

NADS - NAD Synthase

NADP - Nicotinamide Adenine Dinucleotide Phosphate; NADP refers globally to the oxidized ($NADP^+$) and reduced (NADPH) forms.

NADK - NAD Kinase

NAM - Nicotinamide

NAMN - Nicotinic Acid Mononucleotide

NAMPT - Nicotinamide Phosphoribosyltransferase

NAMPT-L - Nicotinamide Phosphoribosyltransferase-like

NAPRT - Nicotinic Acid Phosphoribosyltransferase

NFK - *N*-formylkinurenine

NHD - Nudix Homology Domain

NMN - Nicotinamide Mononucleotide

NMNAT - Nicotinamide Mononucleotide Adenylyltransferase

NR - Nicotinamide Riboside

NMRK - Nicotinamide Riboside Kinase

PARP - Poly-(ADP-ribose)-polymerase

PBEF - Pre-B-cell colony-enhancing factor

PBS - Phosphate Buffer Saline

PER2 - Period Circadian Protein

PERK - Protein kinase RNA like ER kinase

PFA - Paraformaldehyde

PGP - Glycerol-3-phosphate Phosphatase

PI - Propidium Iodide

PQC - Protein Quality Control

PRPP - 5-phosphoribosyl pyrophosphate

PTM - Post-translational Modifications

QA - Quinolinic Acid

QPRT - Quinolinate Phosphoribosyltransferase

ROS - Reactive Oxygen Species

RT - Room Temperature

RT-PCR - Reverse Transcription-Polymerase Chain Reaction

SARM1 - Sterile alpha and Toll/interleukin-1 receptor motif-containing 1

SDS - Sodium Dodecyl Sulphate

SE - Standard Error

SIRT - Sirtuin

SNP - Single Nucleotide Polymorphism

SSC - Side Scatter

TIR - Toll/interleukin-1 Receptor

TOD - Tryptophan 2,3-dioxygenase

TRP - Tryptophan

U - Units

UPR - Unfolded Response Protein

UPR^{mit} - Mitochondrial UPR

UPR^{ER} - Endoplasmic Reticulum UPR

UPS - Ubiquitin Protein System

3-HANA - 3-hydroxyanthranilic acid

3-HK - 3 - hydroxykynurenine

INTRODUCTION

1. Nicotinamide Adenine Dinucleotide (NAD)

1.1 Biological role of NAD

NAD is a pyridine with an essential role in the catabolism of nutrients within cells and is very important for sustaining cellular energy metabolism [1]. This molecule was discovered in the 20th century, around 1906, in seminal studies by Arthur Harden and William John Young. In their experiments, they observed a low molecular weight substance that was present in a boiled yeast extract that accelerated fermentation and alcohol production *in vitro*, and they named this unidentified factor, "cozymase". Around 1930s, Hans von Euler-Chelpin identified the chemical composition of a co-enzyme that consists of two covalently joined mononucleotides, nicotinamide mononucleotide (NMN) and adenosine monophosphate (AMP). In subsequent years, Otto Warburg identified the capability of this molecule to act as a hydride-acceptor and donor in oxidation-reduction (redox) reactions, suggesting that NAD presents two states: the oxidized form (NAD^+) and the reduced form (NADH) [2-4]. In redox reactions, both NAD^+ and NADH are needed and this is key in numerous metabolic pathways, such as oxidative phosphorylation, glycolysis, β-oxidation, tricarboxylic acid cycle [5].

The NAD pool also encompasses other molecules, such as $NADP^+$ (nicotinamide adenine dinucleotide phosphate) and its reduced form, NADP(H). NADP(H) is produced by NAD kinases (NADKs) through addition of a phosphate group. These molecules are important in cellular defence against oxidative stress, synthesis of fatty acids, cholesterol and nucleic acids [2, 6]. NAD and its analogue NADP are involved in catabolic and anabolic, as well as, in aerobic and anaerobic reactions [4]. In the KEGG database (http://www.genome.jp/kegg/pathway.html) these metabolites are implicated in more than 1000 reactions and both redox couples are essential for maintaining the biological processes. Thereby, loss of redox homeostasis is associated with several pathologies, such as cardiovascular diseases, cancer, neurodegenerative diseases and aging [7].

More recently, NAD was identified as a co-substrate for three classes of enzymes, called NAD-dependent enzymes that present distinct roles in the cell: (i) the sirtuins (SIRT1 to SIRT7, in mammals), (ii) the poly(ADP – ribose) polymerases (PARPs) and ADP-ribosyltransferases (ARTs), and (iii) the cyclic ADP-ribose synthases and ADP-ribosyl cyclases (CD38 and CD157) [8]. These enzymes, through NAD consumption, are involved mainly in non-oxidoreduction pathways, such as DNA repair, Ca^{2+} signalling, proliferation or apoptosis [9-11]. Sirtuins remove acetyl and malonyl groups from histones and transcription factors and are different in tissue specificity, subcellular localization, activity and targets. They are involved in different physiological processes from aging

to inflammation and apoptosis [12]. PARPs and ARTs are a family of enzymes that transfer ADP-ribose groups to target proteins and they are involved in DNA repair, gene expression and regulation [13]. CD38 and CD157 are transmembrane proteins that use NAD as a substrate to generate Nam and Ca^{2+}-mobilizing messengers such ADP-ribose (ADPR) [14]. CD38 can also generate cyclic ADP-ribose (cADPR) from ADPR [15]. Another NAD-consuming enzyme called SARM1 (sterile alpha and Toll/interleukin-1 receptor motif-containing 1) was discovered that is present in the outer mitochondrial membrane. The TIR (Toll/interleukin-1 receptor) domain of SARM1 has catalytic activity (NADse) to cleave NAD [16, 17]. SARM1 promotes axonal degeneration through NAD depletion in response to mitochondrial toxins, nerve injury or oxygen deprivation and, therefore, links loss of NAD and Wallerian degeneration [18, 19].

The latest discovery about NAD was the identification of a new role as a regulator of protein-protein interactions through NHDs (Nudix homology domains) that have no known function. It was suggested that binding of NAD to the NHD domain of DBC1 (deleted in breast cancer 1) prevents it from inhibiting PARP1. In cancer and aging, DBC1 is increased resulting in the formation of more DBC1-PARP1 complexes. These complexes reduce DNA repair and increase DNA damage. Therefore, supplementation with NAD or its precursors in old mice, appears to protect against cancer and aging through a negative-feedback loop that prevents the binding of DBC1 to PARP1 [20].

1.2. NAD biosynthesis pathways

As a universal and essential coenzyme, NAD is one of the most abundant molecules in living cells [21, 22]. Intracellular NAD levels are regulated by a balance between synthesis and degradation processes, where multiple enzymes are involved [23]. NAD can be produced from different pathways, the amidated route that comprises the *salvage* pathways and the deamidated route or *de novo* pathway [22, 24]. NAD biosynthesis is different between vertebrates and invertebrates and some species are incapable of synthesizing NAD *de novo,* therefore, rely on external NAD and/or salvage pathways from different precursors [25]. The main precursors used by mammals to synthesize NAD include tryptophan (Trp) in the *de novo* pathway and, in the *salvage* pathways, nicotinamide (Nam), nicotinamide riboside (NR) and nicotinic acid (NA). Nam, NR and NA are three forms of niacin, or vitamin B_3 (Figure 1) [26]

A well-known route to NAD is the Preiss-Handler pathway. First, NA is converted into nicotinic acid mononucleotide (NaMN) through addition of ribose-phosphate by nicotinic acid phosphoribosyltransferase (NAPRT), the rate-limiting enzyme in this pathway. Then, nicotinamide

mononucleotide adenylyltransferase (NMNAT) converts NaMN into nicotinic acid adenine dinucleotide (NAAD) in the presence of adenosine triphosphate (ATP), and, finally, NAAD generates NAD through addition of an amino group by NAD synthase (NADS) (Figure1) [27, 28].

The *de novo* pathway is also called the deamidated route or kynurenine pathway. The first step is the rate-limiting step in the pathway and consists in the oxidation of Trp to *N*-formylkinurenine (NFK) by indoleamine 2,3-dioxygenase (IDO) or tryptophan 2,3-dioxygenase (TDO). Then, kynurenine is converted into 3-hydroxykynurenine (3-HK) or anthranilic acid (ANA). These molecules are then oxidized into 3-hydroxyanthranilic acid (3-HANA) to generate 2-amino-3-carboxymuconic-6-semialdehyde (ACMS). This last component is converted into quinolinic acid (QA) and then QA is transformed in NaMN by quinolinic acid phosphoribosyltransferase (QPRT). Ultimately, NaMN is adenylated into NAAD which is amidated to form NAD through the Preiss-Handler pathway (Figure 1) [28-30]. However, in mammals tryptophan alone is insufficient to support physiological NAD levels and therefore the *salvage* pathways sustain the intracellular NAD production in several tissues [31].

The main *salvage* pathway is a two-step process in which nicotinamide generated by NAD-consuming proteins is recycled to maintain NAD levels. Nicotinamide phosphoribosyltransferase (NAMPT) and nicotinamide mononucleotide adenylyltransferase (NMNAT) are the enzymes involved. NAMPT is the rate-limiting enzyme and can be intracellular (iNAMPT) or extracellular (eNAMPT). In mammals NMNAT has three isoforms identified (NMNAT-1, 2 and 3) with different properties and cellular localizations: nucleus, the Golgi complex and mitochondria, respectively [32]. The first step of this pathway is the combination of nicotinamide with 5-phosphoribosyl pyrophosphate (PRPP) by NAMPT to generate nicotinamide mononucleotide (NMN). Then, NMN is adenylated by NMNAT in presence of ATP to produce NAD [24, 30, 33]. Nicotinamide riboside, which is obtained from milk, is another precursor of the *salvage* pathways [34]. In this route, NR is converted into NMN by human nicotinamide riboside kinase 1 and 2 (NMRK-1 and NMRK-2). Then, NMN is transformed into NAD through the action of NMNATs. *NMRK-1* is ubiquitously expressed in mammalian tissues while *NMRK-2* is an inducible form highly expressed in the muscle (Figure 1) [15].

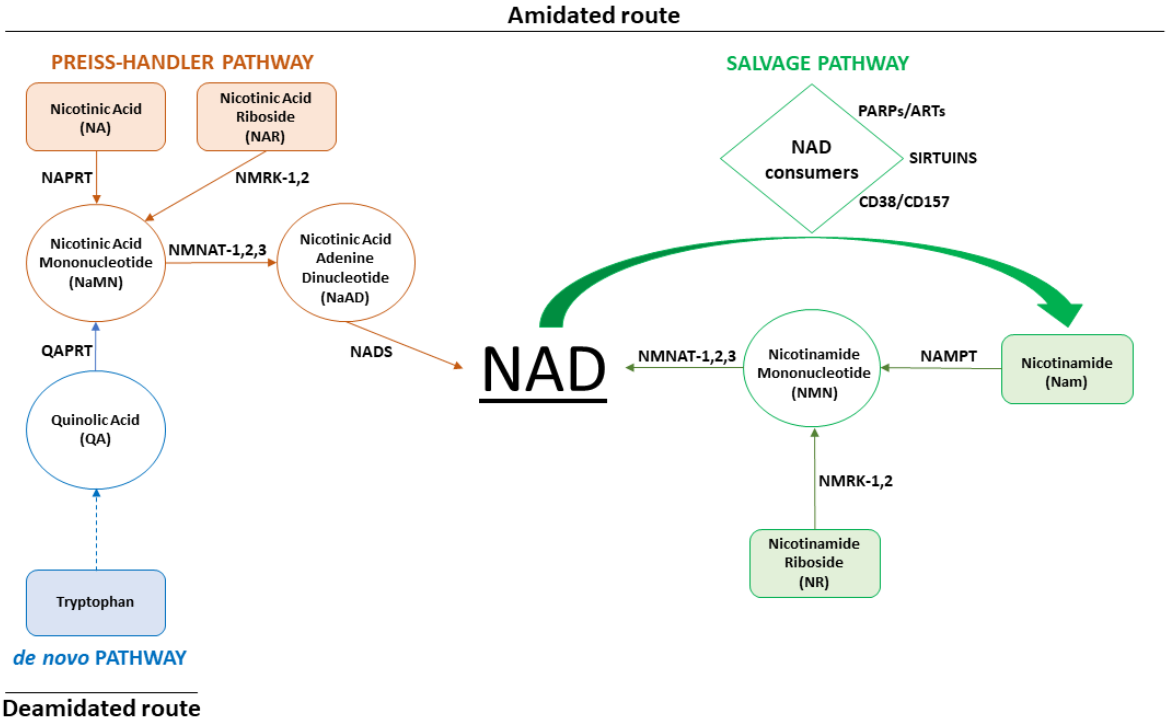

FIGURE 1. MAMMALIAN NAD BIOSYNTHESIS PATHWAYS.

In the *de novo* pathway tryptophan is converted into quinolinic acid, which is then converted to nicotinic acid mononucleotide by quinolinic acid phosphoribosyltransferase. In the *salvage* pathways nicotinamide is converted into NMN by nicotinamide phosphoribosyltransferase while nicotinamide riboside is converted into NMN by nicotinamide riboside kinase. In the Preiss-Handler pathway, NAD is obtained from NA by nicotinic acid phosphoribosyltransferase (Adapted from G. Sultani *et al.*, 2017). Filled rectangles represent the NAD precursors and empty circles represent NAD intermediates. Discontinuous arrow represents other steps in this pathway.

2. Nicotinamide Phosphoribosyltransferase (NAMPT)

NAMPT ubiquitous expression suggests pleiotropic functions in human physiology [35, 36]. The enzymatic activity of NAMPT was originally reported in 1957 by Preiss and Handler [26]. Around 1994, it was identified as pre-B-cell colony-enhancing factor (PBEF) that is a cytokine that enhances the maturation of B-cell precursors. Later, it was identified as visfatin, an adipokine that has increased expression in obesity [37]. The gene encoding NAMPT was identified only in 2001 in *Haemophilus ducreyi* and after that, many groups described NAMPT as a dimeric type II phosphoribosyltransferase [38, 39]. The human *NAMPT* gene is localized at chromosome locus 7q22.3 [40] and has around 3000 SNPs (Single Nucleotide Polymorphisms) reported, but only a small fraction of these SNPs is deleterious and is involved in pathological conditions (www.ensembl.org) [41]. Knockout of NAMPT in female mice is lethal, while heterozygous mice

showed impaired glucose tolerance due to a defect in glucose-stimulated insulin secretion and due to the reduced plasma levels of eNAMPT and NMN [22, 38].

The protein has 491 amino acids with a molecular weight of 53KDa [40] and can be intra or extracellular. iNAMPT is expressed in almost all organs, tissues and cells [40] and, although it is unclear which cell type or tissue are the main sources of eNAMPT, adipose tissue and hepatocytes contribute to circulating NAMPT levels [42]. eNAMPT has also been found in human and mouse circulation, as well as in human cerebrospinal and seminal fluids [35]. Some studies demonstrated that eNAMPT has higher NAD biosynthetic activity than iNAMPT, while other studies indicate that eNAMPT might function as a growth factor [35]. The mechanism or the stimuli that promote NAMPT secretion has been discussed and investigated. A molecular study reported that iNAMPT undergoes post-translational modifications (PTMs) [43] and is deacetylated specifically at lysine 53 by SIRT1, promoting eNAMPT release (non-classical pathway) [35, 44]. Besides, in the literature the experimental conditions that do not lead to cell death, but represent a strong stress for cell, such as nutritional changes, cellular stress and inflammatory signals, trigger the release of eNAMPT in many cell types, including SH-SY5Y cells [43, 45].

Due to the different functions of NAMPT, this protein is involved in several pathologies, such as metabolic, cardiovascular and immune disorders and cancer. NAMPT overexpression has been reported in several tumours, including breast and thyroid cancers, glioma and melanomas and these high levels are associated with a poor prognosis in some cases, such as glioblastoma. In hematopoietic cancers, mainly in lymphomas, NAMPT levels are also increased, suggesting that eNAMPT can have an important role in cancer development [40]. Circulating NAMPT has also been associated with obesity, non-alcoholic fatty liver disease and type 2 diabetes while underexpression of intracellular NAMPT has been associated with aging [8].

2.1. NAMPT and the Circadian Clock

Circadian rhythm is an important regulator of NAD content and regulates the transcription of the intracellular form of NAMPT, mainly located in the nucleus and cytoplasm. The key mammalian circadian regulators are the Circadian Locomotor Output cycles Protein Kaput (CLOCK) and Aryl Hydrocarbon Receptor Translocated – Like protein 1 (BMAL1) [2, 46]. This endogenous clock allows the adaptation of organisms to the Earth´s rotation and is present in all mammals in the Hypothalamic Suprachiasmatic Nucleus (HSN). The function of circadian clock genes is mainly regulated by sirtuins, therefore appropriate NAD levels are necessary. SIRT1 interacts with CLOCK that heterodimerizes with BMAL1, forming a complex that promotes the activation of circadian

clock genes and NAMPT expression. SIRT1 also interacts with and deacetylates PER2 (Period Circadian Protein), which heterodimerizes with other protein and inhibits the CLOCK:BMAL1 complex [47, 48]. In wild-type mouse liver and adipose tissues, the expression levels of NAMPT RNA and protein are higher at diurnal period and lower in dark period. Liver NAD levels showed the same oscillation, suggesting that the clock system is required to regulate NAMPT expression and NAD availability [49]. Therefore, NAMPT/SIRT1/CLOCK:BMAL1 act in a feedback loop with the light-dark cycle, in which NAMPT contributes to NAD biosynthesis. NAD will be consumed by sirtuins to activate the complex CLOCK:BMAL1 and once activated, the complex promotes the expression of NAMPT, resulting in increased NAD levels (Figure 2) [35]. Any decline in circadian function would affect the temporal order of metabolism, which may contribute to deterioration in health [3].

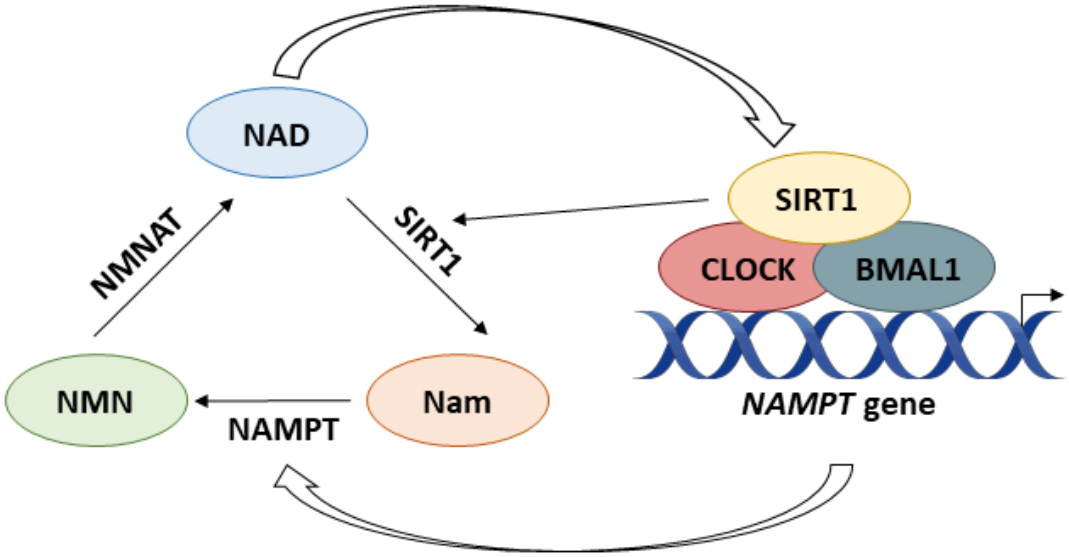

FIGURE 2. THE FEEDBACK LOOP BETWEEN NAMPT/SIRT1/CLOCK:BMAL1.

NAMPT, the main enzyme in *salvage* pathway, contributes to NAD levels and is regulated by circadian regulators, the complex CLOCK:BMAL1. NAD acts as a substrate for many enzymes, such as SIRT1., SIRT1 binds to CLOCK and deacetylates BMAL1, and this complex regulates NAMPT expression and, consequently, NAD availability (Adapted from Wang *et al.*, 2016).

2.2. NAMPT and tissue communication

There are tissues and organs that do not have adequate amounts of iNAMPT and therefore rely on circulating NMN and other NAD intermediates. The fact that NMN could be synthesized and then distributed to all body, suggest that exogenous NMN is a circulating signalling molecule for organs or tissues [38]. Besides NAD biosynthesis, NAMPT acts as an adipokine, and it has been suggested that adipose tissue connects other tissues as an endocrine organ, regulating NAD production at a systemic level in mammals [43, 44]. Adipose tissue-specific *NAMPT* knockout (ANKO) mice have

decreased circulating eNAMPT levels and hypothalamic NAD, reduced SIRT1 activity as well as reduced insulin secretion by pancreatic β-cells. On the other hand, female mice with adipose tissue *NAMPT* knock-in (ANKI) present high levels of hypothalamic NAD, SIRT1 activity and neuronal activity [38, 45, 50].

In this way, NAD metabolism associates tissues with different biological functions, including circadian rhythm and aging control. NAMPT-mediated NAD biosynthesis decreases with age in multiple organs, such as adipose tissue, skeletal muscle, brain and liver, resulting in lower SIRT1 activity and decreased insulin secretion by pancreatic β-cells. Moreover, with age an accumulation of nuclear DNA damage occurs, resulting in chronic activation of PARPs that accelerate NAD depletion and further decreasing the activity of sirtuins [38, 50]. Xeroderma pigmentosum (XPA) is a consequence of the chronic activation of PARP1 [2]. As pancreatic β-cells and the brain start having functional problems due to insufficient NAD levels, other peripheral tissues and organs would also be affected, resulting in the gradual deterioration of the physiological body robustness. In 2009 the "NAD World" concept was suggested that integrates the network for the regulation of NAD metabolism, biological rhythm, and aging [51]. In 2016 the concept was reformulated with an emphasis on the inter-tissue communication between key organs, namely, the hypothalamus, the skeletal muscle and the adipose tissue. The hypothalamus as a control centre for aging, the adipose tissue as a modulator of NAD levels through eNAMPT release, and the skeletal muscle as an effector [2, 50].

Several studies in mammalian cell lines and mice showed that the administration of NAD precursors, such as nicotinamide mononucleotide and nicotinamide riboside increase NAD levels and SIRT1 activity improving mitochondrial and muscle function. Furthermore, chemical inhibitors of PARPs increase NAD levels and, consequently, increase lifespan [52, 53]. It has also been demonstrated that NMN ameliorated some disorders, such as Alzheimer Disease and type 2 diabetes [50]. However, which is the better compound to improve or ameliorate healthspan is not known yet.

3. Protein Aggregation

Protein homeostasis, the balance between protein production and degradation, is very important for cell survival and cell proliferation. Proteins are translated in the Endoplasmic Reticulum (ER)-associated ribosomes, folded inside the ER lumen and trafficked to the Golgi Complex. Besides protein translation, ER acts as a Ca^{2+} storage and is involved in gluconeogenesis and phospholipid biosynthesis. This organelle contains a large range of proteins, including chaperones,

oxidoreductases, holdases and foldases that participate in protein folding, post-translational modifications and protein quality control to obtain functional proteins.

A protein is correctly folded if it has attained its three-dimensional native structure (3D-structure) after the required co- or post-translational modifications (PTM) [54, 55]. The unfolded and misfolded proteins, as well as native proteins that undergo unfolding, contribute to the formation of free radicals and reactive oxygen species (ROS) leading to cytotoxicity, in a positive feedback loop, specially under stress conditions [56]. Misfolded and unfolded proteins can interfere with normal cellular functions. To maintain proteostasis, several regulatory and control pathways are available to minimize homeostasis perturbations – Protein Quality Control (PQC). These surveillance mechanisms include ER-Associated Degradation (ERAD), the Ubiquitin-Proteasome System (UPS), autophagy, heat-shock response (HSR) proteins and chaperones, and the Unfolded Protein Response (UPR) [56-60]. These pathways have been mainly characterized in the cytoplasm, mitochondria and ER.

Molecular chaperones occur ubiquitously in all cellular compartments that sustain protein synthesis and folding reactions. They can interact with nascent amino acid chains or are involved in guiding later stages of the folding mechanisms. They can also rescue misfolded and aggregated proteins and enable them to fold correctly, increasing the efficiency of the overall process by reducing the probability of aggregation [61, 62].

Cellular proteins that are unable to fold properly, non-functional protein fragments and no longer useful proteins, are targeted for degradation by a proteolytic mechanism, namely the Ubiquitin Proteasome System. The 26S proteasome is a large protein complex composed by the 20S proteasome and a regulatory complex, the 19S proteasome cap. It mediates degradation of cytosolic, nuclear, secretory and transmembrane proteins, short-lived and soluble unfolded or misfolded proteins. Ubiquitin serves as a degradation signal for target proteins and polyubiquitinated proteins are degraded in an ATP-dependent process [63, 64]. First, a chain of several copies of ubiquitin binds to lysine residues of proteins through the action of a network of E1 (ubiquitin-activating), E2 (ubiquitin-conjugating) and E3 (ubiquitin ligase) proteins. Then, the ubiquitin chain must be matured and recognized, and the last step is the degradation within the proteasome. After degradation, autophagy is activated to remove the generated “waste” and to remove other proteins that escaped from degradation. This process promotes cell survival also by providing energy via recycling cellular components [65]. The Ubiquitin Proteasome System is involved in the regulation of several cellular processes, such as transcription, cell cycle progression,

cell stress response and apoptosis. For example, to allow the progression of the cell cycle, cyclins and the anaphase-promoting complex (APC) must be degraded by the proteasome [66, 67].

Unfolded Protein Response is a mechanism that occurs in the endoplasmic reticulum (UPR^{ER}) and mitochondria (UPR^{mit}) and they can act alone or overlap to produce protective effects [60]. The first one is activated when ER stress occurs and once activated, leads to the upregulation of genes that encode chaperones and heat-shock proteins, inhibition of protein translation and initiation of ER-Associated Degradation (ERAD) to improve cellular homeostasis [54, 68]. In mammalian cells the UPR^{ER} is activated by three ER transmembrane proteins: activating transcription factor 6 (ATF6), inositol-requiring enzyme 1 (IRE1α) and protein kinase RNA like ER kinase (PERK) that are activated by glucose-regulated protein 78 sensor (GRP78) [69]. These pathways contribute to avoid fatal ER stress through the activation of ER chaperones and the ERAD system [70]. The role of mitochondria in protein aggregation is supported by studies in worms and mammalian cells that showed that UPR^{mit} acts as a transcriptional response promoting folding, limiting import and reducing translation of mitochondrial proteins. UPR^{mit} is activated in response to excessive ROS, amino acid depletion, and ER stress. Besides intracellular UPR^{mit} regulation, UPR^{mit} signalling also occurs between cells and tissues [71].

Proteostasis is influenced by factors such as age, mutations, stress or infections that exceed the capacity of protein quality control, promoting the formation and accumulation of insoluble protein aggregates [72]. These aggregates are abundant in many age-related diseases, mainly in neurodegenerative diseases, such as Alzheimer and Parkinson, and the amount of aggregates increases during aging through proteasome activity decline. Besides the brain, organs such as lungs (chronic lung disease), liver (alcoholic liver disease) and pancreas (type II diabetes mellitus) are also affected [59, 63].

3.1. Protein aggregation and NAD metabolism

Organisms are affected constantly by intrinsic factors such as loss of proteostasis or cellular damage, as well as by extrinsic factors like lifestyle and environmental factors. These stressors lead to a systemic and progressive functional decline, called aging [63]. Unresolved ER and mitochondrial stress, or the accumulation of different types of aggregates in organs and tissues promote cell cycle arrest and apoptosis, contributing to lifespan decrease and aging. Thus, aging *per se* is not defined as a disease, but as a breakdown of biological robustness [50, 56].

In several degenerative diseases and others age-related diseases, such as diabetes, cancer and cardiovascular diseases, specific proteins have been found to misfold, aggregate and form pathogenic assemblies, ranging from small oligomers to large masses of amyloid protein. The aggregated proteins may gain a toxic function and/or lose their normal function promoting the pathology [68, 73]. In mammals, several mechanisms regulate aging, including the insulin-forkhead box protein O (FOXO), mechanisms target of rapamycin (mTOR) pathways and insulin/insulin-like growth factor 1 signalling [50, 74]. These may be related with NAD metabolism as shown in Figure 3 [8, 43].

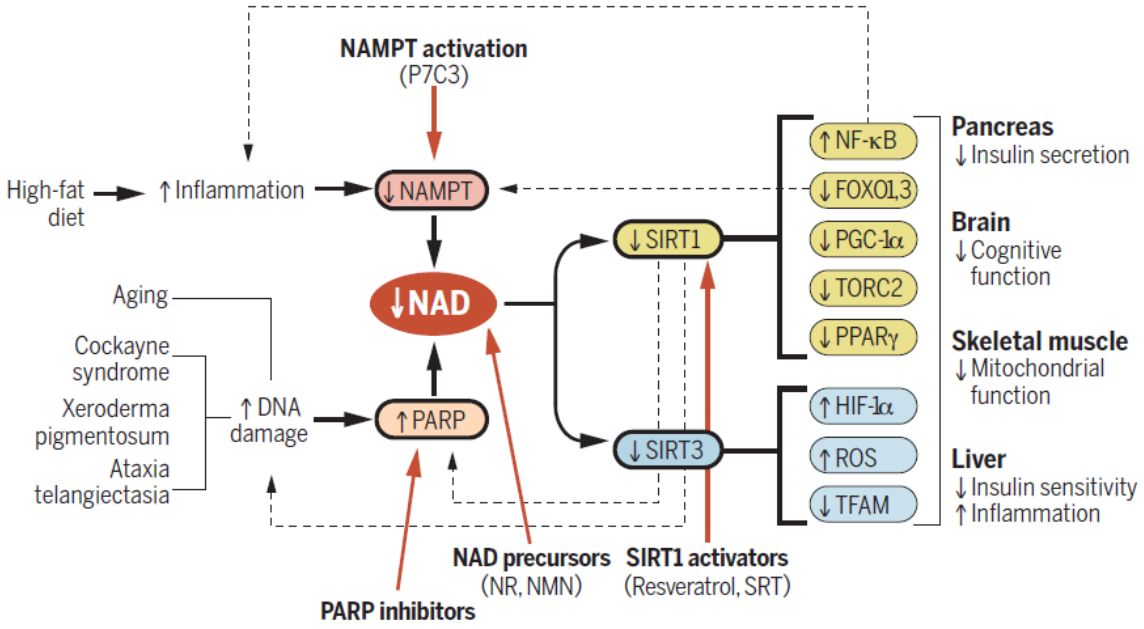

FIGURE 3. A MODEL FOR DNA DAMAGE, INFLAMMATION, NAD AND AGING.

The activation of PARP by DNA damage and the decreased NAMPT expression, lead to decreased sirtuins activity in the nucleus and mitochondria, which is associated with further PARP activation and increased DNA damage. Mitochondrial function is diminished as result of decreased sirtuins activity. Possible therapeutic interventions to restore NAD levels are illustrated by red arrows (From Verdin *et al.*, 2015).

Some studies showed that NAD levels are decreased mainly in neurodegenerative disorders, including Alzheimer and Parkinson diseases. These diseases are characterized by the presence of multiple protein aggregates, such as Aβ plaques and Tau tangles, and mitochondrial dysfunction. NMN supplementation appears to ameliorate cognitive function through restoration of NAD and ATP levels, while NR supplementation reduces Aβ plaques formation in the cortex and hippocampus of mouse [75, 76]. In a long-term study, mice with age-associated pathologies were supplemented with NMN and present reduced weigh, better insulin sensitivity and better physical activity [77].

NMN supplementation successfully improves defects associated to aging and pathologies-associated to aging, indicating that *salvage* pathway decreases with age [8]. Supplementation with NR appears to improve mitochondrial function and muscle strength in aged mice as well [78]. Increasing the activity of enzymes that participate in the *salvage* pathway, such as NAMPT, or using inhibitors for NAD-consuming enzymes can also be a strategy to improve NAD levels during aging [79]. *NMNAT-2* transcript levels, the NAD biosynthesis enzyme that uses NMN as a substrate, are negatively correlated with cognitive dysfunction and Alzheimer disease. Also, SNPs located downstream of the *NMNAT-3* gene are associated with late-onset AD [80]. Besides, NMNAT-2 supresses Wallerian degeneration [80] and tau-induced degeneration [81] through clearance of misfolded proteins and aggregates. is result has been reported in different models of neurodegenerative diseases, in which NMNAT acts as a chaperone interacting with proteasome for neuronal protection [82]. A study in *S. cerevisiae* models of human proteinopathies demonstrated that NMA1/2 (NMNAT homologues) are overexpressed in these models. This overexpression supresses polyglutamine and α-synuclein-induced cytotoxicities, through the clearance of the non-native proteins in large aggregates, decreasing the insoluble aggregates [83]. Studies in *Drosophila* demonstrated the induction and recruitment of NMNAT upon aggregate formation. It has also been demonstrated that the redistribution of over-expressed NMNAT and co-localization at intracellular aggregates may act in concert or in parallel with Hsp70 through the proteasome-mediated pathway [82]. Other NAD *salvage* enzymes in yeast, such as NPT1, QNS1 and PNC1 also present protective effects [83] as well as the human homologue hsNMNAT-3 that displays chaperone activity to the *Drosophila* proteins [82].

In the last years, many progresses have been done in the study of NAD metabolism to improve human aging and reverse pathological phenotypes, however which is the better strategy is still unclear [11]. Thus, the aim of the present study is to investigate the role of NAD metabolism in protein aggregation in SH-SY5Y cells, as well as to investigate if NAD or its precursors could ameliorate protein aggregation.

OBJECTIVES

Aims of the study

Several studies show that protein aggregation and its accumulation are a trigger to aging-related diseases, such as Alzheimer and Parkinson diseases [84]. NAD levels decrease with age in yeast and mice. In human tissues, this depletion has also been reported in several tissues, such as pancreas, brain, skeletal muscle and liver and are implicated in several diseases, mainly neurodegenerative diseases [76]. However, the relation between NAD depletion, protein aggregation and neurodegeneration is yet unclear.

Thus, the main goal of this study was to investigate if and how protein aggregation is correlated to NAD metabolism. The specific aims were:

- To investigate the cell viability and cell metabolic state in response to the proteasome inhibitor MG132 and the NAMPT inhibitor FK866;
- To investigate the effect of MG132 and FK866 in protein aggregation;
- To evaluate the expression of NAD biosynthetic enzymes under stress conditions (MG132, FK866 and both inhibitors);
- To investigate the effect of NAD precursors in protein aggregation in the presence of proteasome and NAMPT inhibitors.

Overall, our study elucidates the importance of NAD metabolism in protein aggregation in SH-SY5Y cells.

METHODS

1. Cell Culture

In this thesis the human neuroblastoma cell line (SH-SY5Y) was used, obtained from the iBiMED cell culture bank. SH-SY5Y cells were routinely cultured in MEM:F12 medium supplemented with 10% FBS and 1% (100U/mL) of streptomycin, penicillin and amphotericin solution at 37°C with 5% CO_2 in a humidified atmosphere. Cells were seeded in 10øcm culture dishes and split when confluent.

Confluent cells were washed with 1xPBS and incubated 5 minutes with 2mL trypsin-0,5% EDTA at 37°C to detach the cells. After incubation, 4mL of culture medium was added to dishes to block the action of trypsin. Cells were resuspended in the medium and centrifugated at 1000rpm (Heraeus™ Multifuge™ X1R Centrifuge, Thermo Scientific) for 3min at room temperature (RT). Finally, cells were divided according to experimental needs and/or seeded at a 1:10 dilution (≈100 cells/mL).

Cells stocks were prepared from confluent cells resuspended MEM:F12 medium supplemented with 5% DMSO and were kept in cryovials as aliquots of 1mL. Stocks were placed in the liquid nitrogen tank (flash-frozen) for cryopreservation.

When needed, frozen cells were thawed through resuspension in 1mL pre-warmed culture medium, centrifugated for 3min at 1000rpm (Heraeus™ Multifuge™ X1R Centrifuge, Thermo Scientific) to remove dead cells and DMSO. Cells were seeded in a 10øcm culture dishes.

2. Chemical treatments

For chemical treatments, two million SH-SY5Y cells were placed in fresh medium containing different concentrations of proteasome inhibitor MG132 (5µM and 10µM), NAMPT inhibitor FK866 (10nM, 100nM and 1µM) or both inhibitors simultaneously with different exposure times (1, 2, 4, 8, 16 and 24hours). In addition, cells were treated with NAD (10mM) or NAD precursors (10mM Nicotinamide or 1mM Nicotinamide Mononucleotide, simultaneously or not, with MG132 and FK866 at the same exposure times. DMSO (vehicle) was used as the control treatment. The medium was removed after each incubation and cells were treated to perform the experiments described next.

3. Cell Viability

The morphology, number and adherence of cells were directly observed in the optical microscope before any procedure. Cell viability was measured using a PI (Propidium Iodide) assay, which is based on the entry of PI into dead cells [85]. After treatments, cells were washed with 1xPBS, detached by trypsinization and then centrifugated at 800x*g* for 5min. The supernatant was removed and a total of one thousand cells (counted with a Neubauer chamber, Celoromics) were

resuspended in 1xPBS and immediately stained with 5µL of PI (1mg/mL) in the dark and in ice. Cell death was detected using a BD Accuri™ C6 Cytometer and the data was acquired and analysed using BD Accuri™ C6 Software (BD Biosciences). A negative control (without stain) was used to remove background. Before the analyses, the cell suspension was filtered using a 40µm cell strainer. The analysis was made in the FL-2 region (corresponding to the PI fluorescence intensity, 610nm) and the samples were analysed in typically 300s. The total volume ranged from 30 to 100µL.

4. Cell metabolic state

To evaluate the metabolic state of cells during and after treatments, the resazurin reduction assay was performed. It is a colorimetric method that identifies viable cells through the reduction of resazurin (blue) to resofurin (pink) by mitochondrial dehydrogenases [86]. Resazurin was diluted in 1xPBS to one-tenth of culture volume, added in all different cell treatments and incubated during 2h or 4h at 37°C and 5%CO_2. The compound was added at the beginning and/or at the end of each exposure time (2, 4, 8, 16 and 24h). Fluorescence intensity was measured at 570 and 600nm using a Plater Reader Infinite® 200 PRO (TECAN) and all experiments were carried out in triplicate. Besides treated cells, a positive and a negative control were performed. The positive control corresponds to cells without treatment (maximal viability) and a negative control corresponds to fluorescence of the growth media without cells (zero viability).

Metabolic activity was then calculated using the following formula:

$$\%\text{Viable Cells} = \frac{\text{O.D.treated cells} - \text{O.D.negative control}}{\text{O.D.positive control} - \text{O.D.negative control}} \times 100\%$$

O.D. optical density

FIGURE 4. FORMULA TO CALCULATE THE PERCENTAGE OF VIABLE CELLS.

5. Protein aggregation analysis by Flow Cytometry

To analyse protein aggregation by flow cytometry, SH-SY5Y cells were plated on 6øcm culture dishes at a concentration of $2x10^6$ cells/5mL. After 8h and 24h of incubation with the different chemicals, the cells were washed in 1xPBS and detached with 1mL of trypsin/0,5% EDTA. After 5min of incubation at 37°C and 5% CO_2, 2mL of growth media was added and the trypsin was removed by centrifugation at 800x*g* for 5min. The supernatant was discarded, while the cell pellet was resuspended in 200µL of 1xPBS at a concentration of $1,5x10^6$ cells/200µL.

For analysis by flow cytometry, cells were fixed with 1mL of 4% Paraformaldehyde (PFA) during 30min at room temperature and then were permeabilized with 0,5% Triton X-100/3mM EDTA during 30min on ice. After permeabilization, cells were stained with 200µL of ProteoStat® (1:45000) for 30min in the dark. Between each reagent addition, the cells were centrifugated at 800x*g* for 15min at 4°C to discard the supernatant and then were washed with 1xPBS by centrifugation at the same conditions as before. Flow cytometry was performed using a BD Accuri™ C6 Cytometer and the events were acquired and analysed using the BD Accuri™ C6 Software (BD Biosciences). A negative control (without stain) was used to remove background and before analyses, the cell suspension was filtered using a 40µm cell strainer. The analysis was made in the FL-3 region (corresponding to ProteoStat® fluorescence intensity, 488nm) and viable cells were gated (P1) in the SSC (Side Scatter, corresponding to cell complexity, y axis) versus FSC (Forward Scatter, corresponding to cell size, x axis) plot. For each sample 10.000 events were acquired within the P1, whenever possible and the drawn gates were the same for all conditions in each analysis within the same experiment. Cells present in samples were analysed in typically 300s and the total volume analysed ranged from 50 to 200µL.

6. Protein aggregation analysis by Fluorescence and Confocal Microscopy

Wide-field fluorescence microscopy was performed to visualize protein aggregates. SH-SY5Y cells were plated in 22ømm glass coverslips within 6øcm culture dishes at a concentration of $2x10^6$ cells/5mL. After 8h and 24h of incubation with the different chemicals, the coverslips were transferred to new culture dishes and the remaining cells were kept for protein or RNA extraction.

In the new culture dishes, the coverslips were washed three times with 1xPBS and then were fixed for 30min with 4% PFA at RT. To permeabilize cells, a solution of 0,5% Triton X-100/3mM EDTA was added for 30min at 4°C with shaking, and in the last step the cells were stained with ProteoStat® by incubating for 30min on dark. For this, 60µL of reagent (1:2000) was added to all samples and between each step the cells were washed three times with 1xPBS. After staining, coverslips were washed in ddH_2O, mounted in glass slides with mounting medium with DAPI and dried for 1h in the dark. Glass slides were stored at 4°C until observation under a fluorescence or a confocal microscope.

The cells were observed with AxioImager Z1 Zeiss Microscope and AxioVision Software, using 63.0x1.40 oil objective equipped with the appropriate filter combination. Confocal photos were acquired using Leica TCS SP5 confocal microscope, with 63.0x1.40 oil objectives and analysed using LAS AF (Leica). The lasers used were Diode 405-30 (405nm for DAPI) and DPSS 561-10 (561nm for

ProteoStat®). The images were then analysed using LAS X and ImageJ software. The settings for ProteoStat® analysis were the same in all conditions while the settings for DAPI analysis were changed (i.e. laser power) according to the condition.

7. Gene Expression analysis

Reverse Transcription-Polymerase Chain Reaction (RT-PCR) technique was used to evaluate gene expression. It is a semi-quantitative technique used to measure the expression levels of several target genes from each sample.

Around one million cells plated in 6øcm culture dishes were lysed at room temperature with 300µL of ice-cold TRIZOL. After homogenization, the samples were stored at -80°C or used immediately until further processing. RNA isolation was performed according to the manufacturer instructions of Direct-zol™ RNA MiniPrep (Zymo Research - R2050). All centrifugations were performed at 13000x*g* for 30s. Briefly, equal volume of ethanol was added to samples in TRIZOL and the mixture was homogenized, transferred into a Zymo-Spin™ IIC Column in a collection tube and centrifugated. After, the column was transferred into a new collection tube and the supernatant was discarded. To eliminate genomic DNA contamination, RNA was treated with DNase I. First, 400µL RNA Wash Buffer was added to the columns and centrifugated, then 80µL DNase I (6U/µL) in reaction buffer was added for each sample and incubated for 15min at room temperature.

After DNA elimination, RNA was purified by adding 400µL Direct-zol RNA PreWash to the columns followed by centrifugation. The supernatant was discarded, and this step was repeated. Next, 700µL RNA Wash Buffer was added and the columns were centrifugated at 13000x*g* for 2min to ensure complete removal of the wash buffer. To elute RNA, the column was transferred into a RNase-free tube and 30µL of DNase/RNase-Free Water was directly added to the column and centrifugated. The RNA concentration and purity were measured with Nanodrop (DeNovix) equipment using 1µL of RNA per sample. After, samples were used directly to produce cDNA or stored frozen at -80°C.

RNA was used as template for reverse transcription using SuperScript™ II Reverse Transcriptase and Tetro Cdna Synthesis Kit (Bioline, 65042). Each reaction was prepared in a DNase free PCR microtube and the final volume was 20µL. First, 500ng RNA and NF (Nuclease-free) Water were added to 9µL, plus 1µL of d-NTPs and 2µL random hexamers. The mixture was heated for 5min at 65°C and then 4µL 5x First Strand Buffer, 2µL 0.1M DTT and 1µL RNase inhibitor were added followed by incubation for 2min at 25°C. Finally, 1µL Reverse Transcriptase enzyme was added and

cDNA was synthesized on MyCycler™ thermocycler (BioRad) with the conditions described below (Figure 5). At this point cDNA can be stored at -80°C or used for PCR amplification.

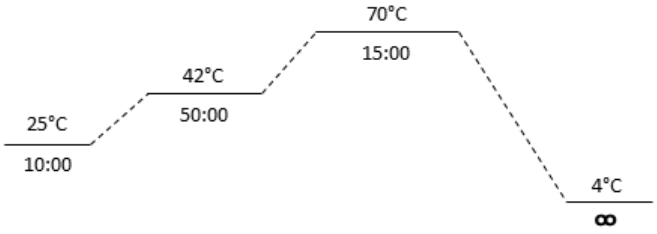

FIGURE 5. CDNA SYNTHESIS.

cDNA was synthesized for 10min at 25°c, followed by 50min at 42°c and the enzyme was inactivated for 15min at 70°c.

cDNA samples were used for target gene amplification using PCR. The genes tested were *NAMPT* and *NAPRT* and expression of the glyceraldehyde 3-phosphate dehydrogenase (*GAPDH*) gene was used as a control in PCR reaction. Reactions were prepared from 1µL of cDNA in a 10µL final volume reaction, using 5µL of HotStarTap® Master Mix, 1µL each primer (final concentration 0,2µM) and Q solution was included in the reaction at 10%. ddH_2O was added to perform the final volume. The samples were amplified in a MyCycler™ thermocycler (BioRad) with the conditions described below:

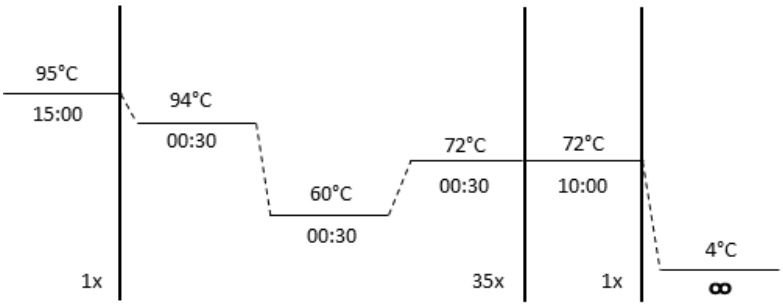

FIGURE 6. PCR CYCLE USED TO AMPLIFY *NAMPT*, *NAPRT* AND *GAPDH* GENES.

The PCR started with an initial denaturation step for 15min at 95°C, followed by 35 cycles of a denaturation – annealing – extension step, and a last final extension for 10min at 72°C.

Agarose gel electrophoresis is a technique that allows separation and purification of PCR fragments of different sizes. Through agarose concentration, it is possible to obtain larger (less agarose) or smaller pores (more agarose), used to separate larger or smaller fragments, respectively [87]. All amplification products were visualized in 1% agarose gels prepared in 130mL 1xTAE. After the molten agarose had partially cooled, 9.75µL GreenSafe Premium® were added and the gel was

poured into the gel tray. Completely set and hardened (≈25min) gel was mounted into electrophoresis chambers and covered with 1xTAE Buffer. Samples for analysis were mixed with 2µL of 5x Nucleic Acid Sample Buffer (loading buffer). Samples were loaded into the sample wells and electrophoresis was carried out at 100V for 30min, using NZYDNA Ladder V to allow sizing. DNA fragments were visualized under UV light and gel image acquisition was processed using GelDoc™ XR^+ (BioRad). The final images were further analysed with ImageLab software.

RESULTS AND DISCUSSION

1. Viability and metabolic state in SH-SY5Y cells

1.1. Cell Viability

The initial step in this study was to evaluate the effect of MG132 and FK866 on SH-SY5Y cell viability. MG132 is a peptide aldehyde that blocks the proteolytic activity of the proteasome complex, promoting protein aggregation [88]. FK866, (E)-N-[4-(1-benzoylpiperidin-4-yl) butyl]-3-(pyridine-3-yl), is a NAMPT inhibitor that promotes delayed cell death [89]. Cells with low passage (ranging from #8 to #13) were treated with different concentrations of MG132 (5µM and 10µM) and FK866 (1µM, 10nM and 100nM) for different periods of time (4h, 8h and 16h). After treatments, cells were immediately stained with 5µL propidium iodide and analysed by flow cytometry. This technique allows a quantitative analysis of cells in suspension, such as counting and sub-populations classification [90]. Propidium iodide (PI) is a fluorescent intercalating agent that binds directly to DNA, which occurs upon membrane damage (late apoptosis), staining only dead cells [85].

Flow cytometry results showed no differences in cell death for the different concentrations of both compounds at all time points (Figure 7).

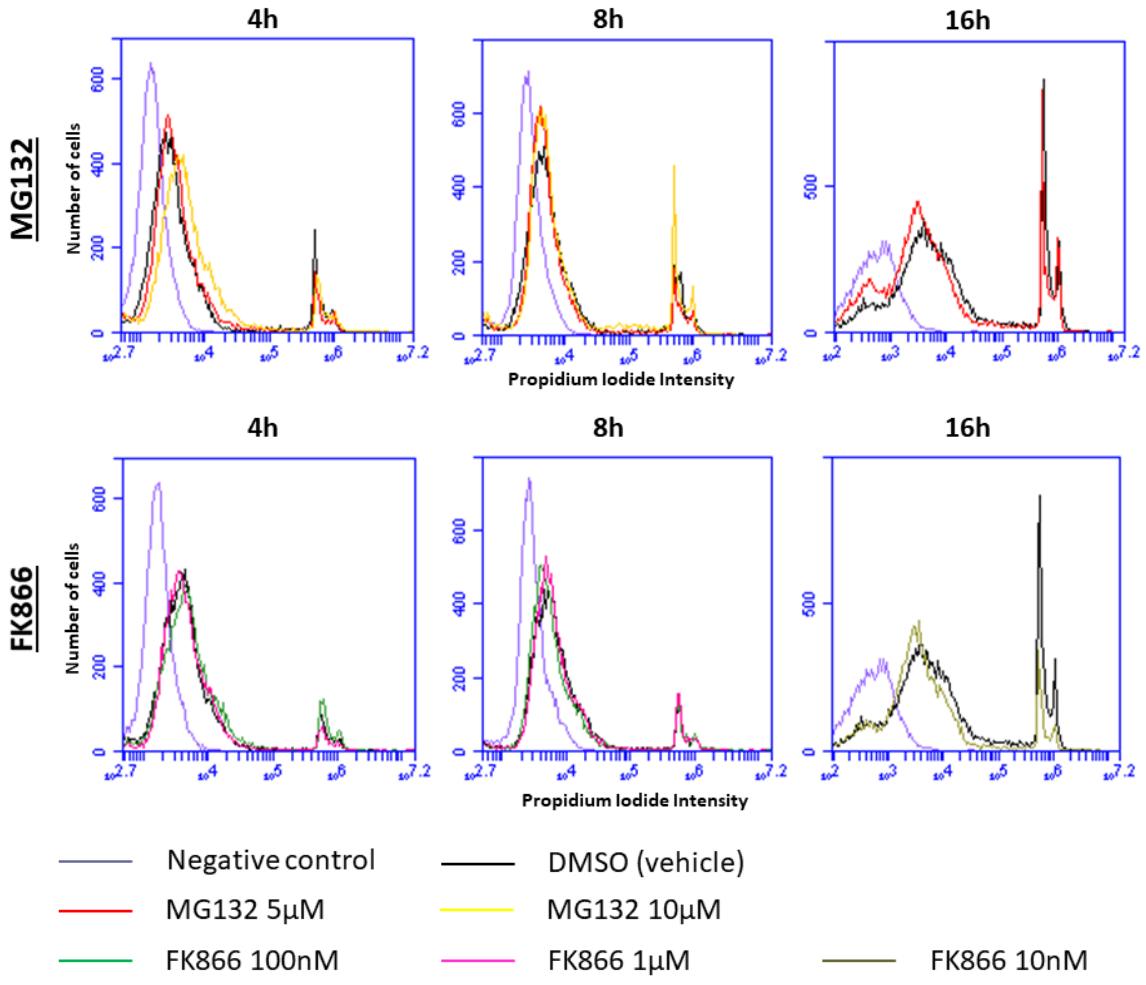

FIGURE 7. CELL VIABILITY IN SH-SY5Y CELLS WITH LOW PASSAGE.

Propidium iodide fluorescence intensity measured by flow cytometry in cells with low passage (ranging from #8 until #13) treated with 5µM or 10µM MG132 and 1µM, 10nM or 100nM FK866 for 4h, 8h and 16h. The left peak in all graphs represents viable cells and the right peak represents dead cells with a total of 10.000 cells.

Dead cells are represented by lines with higher fluorescence intensity (Figure 7). Of note, these lines are overlapping in all times tested and the PI intensity (approximately, 10^6 A.U.) is also identical between time points and chemicals. The viable cells are represented by lines with low fluorescence intensity (10^3 A.U.). Another observation is that at 4h and 8h the number of viable cells is higher than the number of dead cells, but at 16h of treatment the number of dead cells increase while the viable cells decrease. However, at this point, the number of viable cells and dead cells is identical for control and treatment conditions, indicating that treatments do not induce cell death more than control conditions.

These results are according to the literature, because hepatocarcinoma cells treated with 10nM of FK866 showed a decreased viability only after 24h of treatment and cell death was observed at later time [91]. Another recent study showed a decrease in viability only after 40h of exposition with 10nM of FK866 in cancer cell lines with EMT (Epithelial – Mesenchymal Transition) [92]. In our experimental conditions, SH-SY5Y cells treated with FK866, maintain viability for at least 16h (Figure 7). Similarly, for MG132 the number of dead cells increased at 16h, also corroborating the literature. HeLa cells treated with 5µM MG132 presented a 50% decrease in cell viability after 24h of treatment, through cell cycle arrest and loss of mitochondrial membrane potential [88]. Other study showed that U937 leukaemia cells treated with 1µM MG132 present a 20% decrease in viability after 18h of treatment [93]. From our results, we conclude that MG132 in SH-SY5Y cells does not affect viability until 16h of treatment. Otherwise, for longer incubation periods such as cells treated for more than 24h, we expect to see a decrease in viability.

Our results showed that both the proteasome inhibitor and the NAD metabolism inhibitor do not promote more cell death than the control conditions in SH-SY5Y cells with low passage. As PI stains late apoptosis, as alternative we could use Annexin V to stain early apoptosis and distinguish dead cells (late apoptosis) from non-viable cells (early apoptosis), to ensure that the treatments do not influence cell viability [85].

MG132 promotes protein aggregation, and as protein aggregation is the basis of many age-related diseases, we decided to evaluate cell viability in cells with high passage (#30) in response to the

same inhibitors. These cells were treated with 5µM MG132 and 10nM FK866 for 16h. Flow cytometry results are presented in figure 8 and the representative graphs show differences when compared with the results previously described. As above, viability of cells with low passages (Figure 8 A) was not affected by treatments, while in old cells (cells with high passages, Figure 8 B) MG132 (red line) promotes cell death, as the number of dead cells and PI fluorescence intensity are higher than the control (black line). Cells treated with FK866 have the same behaviour than control cells, indicating that a decrease in intracellular NAD levels does not promote cell death until 16h of treatment even in old cells. This effect is the same that occurs in low passage cells, suggesting that decreased NAD levels through NAMPT inhibition are not enough to promote cell death in SH-SY5Y cells until 16h of treatment.

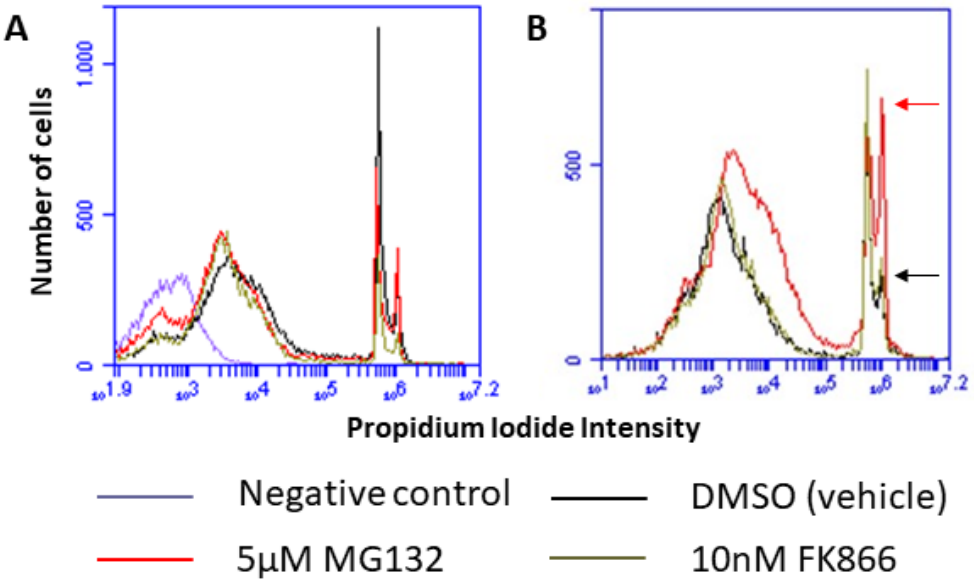

FIGURE 8. CELL VIABILITY IS DIFFERENT BETWEEN CELLS WITH LOW AND HIGH PASSAGE.

Propidium iodide fluorescence intensity measured by flow cytometry in cells with low (#12, **A**) and high (#30, **B**) passage treated with 5µM MG132 and 10nM FK866 for 16h. The left peak in each graph represents the viable cells and the right peak represents dead cells with a total of 10.000 cells. Arrows represent the peak number of untreated cells (black) and MG132 treated cells (red).

1.2. Cell Metabolic State

As the cell viability was not affected by 16h-treatments with chemicals that inhibit the proteasome and the NAD *salvage* pathway, we performed the resazurin assay to measure the cell metabolic state. This assay is based on the reduction of the blue resazurin into pink resofurin. The resazurin reducing capacity of the cells depends on both the activity of mitochondrial dehydrogenases and the amount of the coenzyme NAD(P)H available. Therefore, we can measure indirectly the

intracellular NAD levels, so that a decreased metabolic activity could reflect a decrease in NAD availability.

Cells were treated with 5µM MG132, 100nM FK866 and 5µM MG132 plus 100nM FK866 during 4h, 8h and 24h (Figure 9). MG132 caused a gradual and slight reduction in metabolic state until the end of treatments, while FK866-treated cells, showed an earlier decrease in metabolic state at 8h. At 24h of exposure these cells recovered the metabolic state, almost, to control levels (Figure 9). This could indicate that NAMPT inhibition by FK866 stimulates other pathways to produce NAD (see also chapter 3 below), as already suggested [1] and/or that NAD levels are enough to maintain the metabolic state at 24h. Indeed, a recent study showed that *NAPRT* overexpression in cancer cell lines appears to be protective against FK866-mediated toxicity and is enough to maintain NAD levels [92].

In the treatment with both inhibitors, we observed an early decrease in metabolic activity at 4h (around 40% decrease) that kept constant in longer exposure times (until 24h) (Figure 9). Thus, we conclude that the treatments present a similar trend of a gradual decrease with MG132 and MG132 plus FK866, while FK866 alone promotes an early decrease (8h) followed by a recovery in metabolic state at 24h.

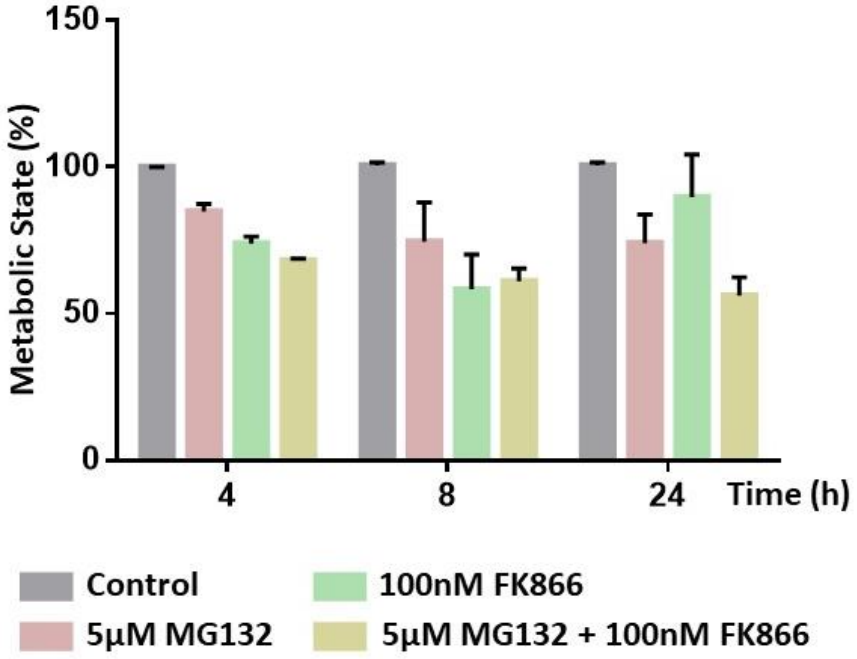

FIGURE 9. METABOLIC STATE IN RESPONSE TO PROTEASOME INHIBITOR (MG132) AND NAMPT INHIBITOR (FK866).

Metabolic state was measured using the resazurin assay in low passage SH-SY5Y cells (ranging from #8 until #13) treated with 5µM MG132, 100nM FK866 and both 5µM MG132 + 100nM FK866 for 4h, 8h and 24h. All experiments were performed in triplicate.

These results are supported by the literature. In HepG2 cells, a decline of dehydrogenase activity only occurred after approximately 3 days of incubation with 10nM FK866 [89]. The same study showed that FK866 treatment did not compromise mitochondrial complex I reactions without a prolonged preincubation (2 days). In U937 leukaemia cells treated with 1µM MG132, a decrease around 40% in mitochondrial membrane potential was reported after 24h, and consequently a decrease in metabolic activity [93], supporting our results.

2. Protein Aggregation in SH-SY5Y cells

We evaluated the effect of different concentrations and different times of exposure to MG132 and FK866 in protein aggregation by flow cytometry. For that, we treated SH-SY5Y cells with 5µM or 10µM MG132 and 1µM, 10nM or 100nM FK866 for 8h and 16h. After treatments cells were fixed, permeabilized and stained with ProteoStat® that contains a novel 488nm-excitable red fluorescent molecular dye that specifically detects denatured and/or misfolded proteins (protein aggregates) within aggresomes. We used as a fluorescence control untreated cells without ProteoStat® to exclude autofluorescence emitted by cell components that emit fluorescence upon 488nm laser excitation. Fluorescence intensity was measured in the FL3 channel and only viable cells were gated (P1 gate), while dead cells were excluded (Figure 10 A). As MG132 promotes protein aggregation, this condition is used as a positive control. Representative histograms from flow cytometry results are presented in Figure 10 B.

Surprisingly, at 8h of exposure, both inhibitors have an identical fluorescence intensity to that of untreated cells (all lines are almost overlapping), which was not expected considering the previous results. After, we increased the exposure time to 16h and tested 5µM MG132 and 10nM FK866, as all concentrations have similar effect in protein aggregation in the earlier time point. Cells treated with MG132 present higher fluorescence intensity (red line) compared to control cells, which means that at 16h of exposure cells present more aggregates than untreated cells, as expected. Additionally, the MG132 fluorescence intensity (MFI – Mean Fluorescence Intensity) is much stronger at 16h than at 8h, suggesting the formation of more aggregates over the time. On the other hand, cells treated with FK866 present fluorescence intensity identical to that of untreated cells (black and green lines are overlapping), indicating that this inhibitor does not promote protein aggregation.

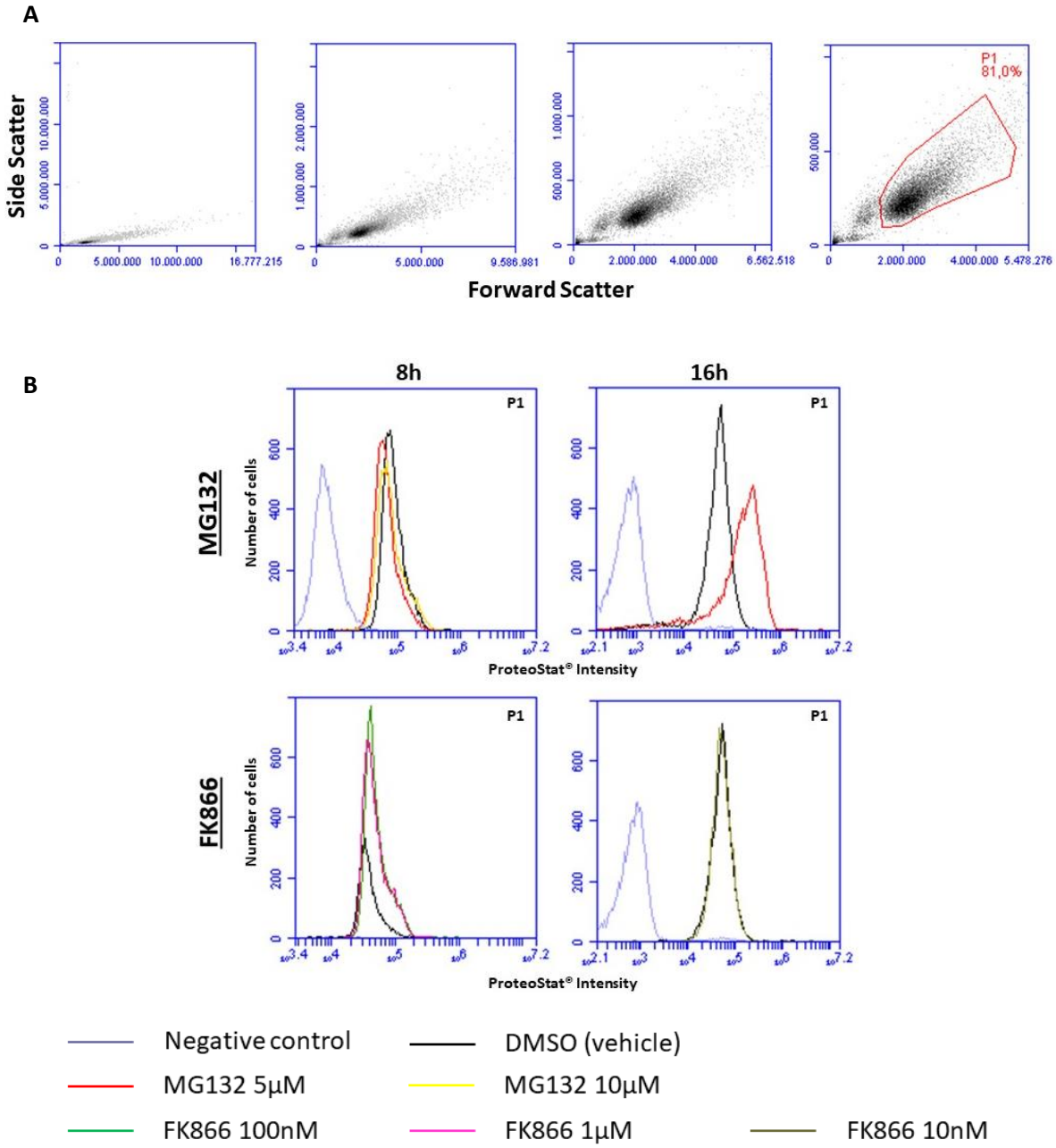

FIGURE 10. PROTEIN AGGREGATION ANALYSIS BY FLOW CYTOMETRY.

A) Representative dot plot of gated viable cells (P1).

B) Representative histograms of ProteoStat® fluorescence intensity measured by flow cytometry in cells treated with different concentrations of MG132 (5 and 10µM) and FK866 (10 and 100nM, 1µM) and different exposure times (8h and 16h). In each graph only, viable cells are represented (P1) with a total of 10.000 cells.

After analysing the effect of both compounds in protein aggregation by flow cytometry, we used confocal microscopy to visualize the aggregates within the cells. SH-SY5Y cells were treated with 5µM MG132, 100nM FK866 and 5µM MG132 plus 100nM FK866 for 8h and 24h. After treatments, cells were stained with ProteoStat® and DAPI to identify the aggregates (red) and the nucleus (blue), respectively. Confocal microscopy results are shown in Figure 11. Control cells (Fig. 11 A) present low red fluorescence, as well as both time points with FK866, at 8h and 24h (Fig. 11 D and E, respectively), indicating that these cells contain identical and small amounts of protein aggregates. On the other hand, cells treated with MG132 present high red fluorescence at 8h and 24h of exposure (Fig. 11 B and C, respectively), supporting the higher MFI obtained by flow cytometry at 16h. An identical result was observed in cells treated with both inhibitors simultaneously, at 8h and 24h, where confocal images showed high red fluorescence corresponding to protein aggregates (Fig 11 F and G, respectively). These results indicate that in SH-SY5Y cells, treatment with the NAMPT inhibitor FK866, which promotes a decrease in NAD levels, does not induce protein aggregate formation in contrast with the treatment with the proteasome inhibitor MG132. When cells are treated with both inhibitors, protein aggregation is also observed.

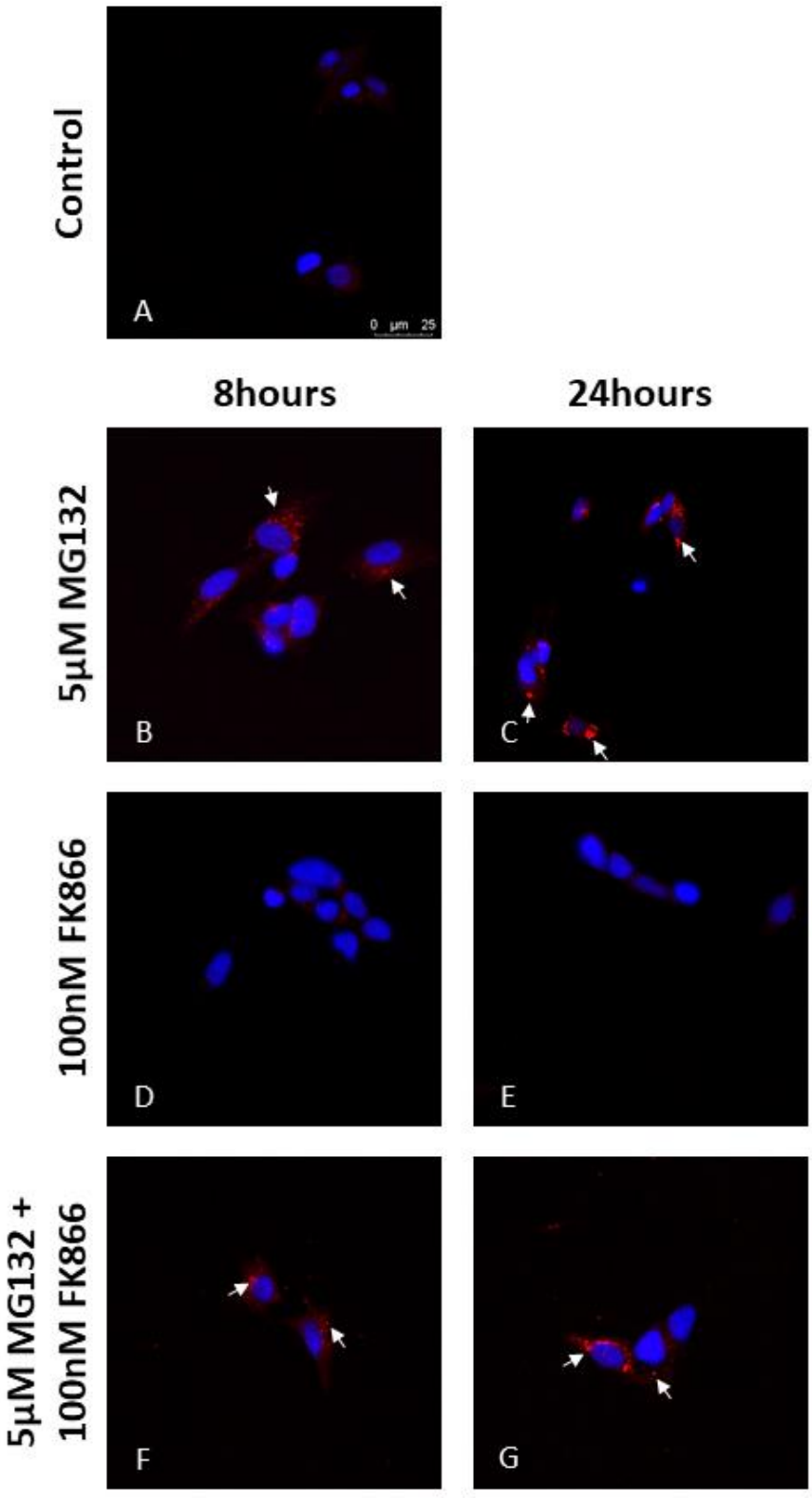

FIGURE 11. PROTEIN AGGREGATION ANALYSIS BY CONFOCAL MICROSCOPY.

Representative confocal images of untreated cells (A); cells treated with 5µM MG132 for 8h (B) and 24h (C); cells treated with 100nM FK866 for 8h (D) and 24h (E); cells treated with 5µM MG132 + 100nM FK866 for 8h (F) and 24h (G). Scale bar represents 25µm and arrows represent protein aggregates.

We also observed that protein aggregates appear to be localized in higher amounts in different intracellular localizations, mainly in the cytoplasm but also in the perinuclear region and nucleus, at a smaller extent. More studies are needed to support this, such as co-localization with organelle markers. In all treatments that promoted protein aggregation, we also observed a gradual increase in red fluorescence over time, suggesting that more protein aggregates are formed (Figure 11). To evaluate this increase, one hundred cells were randomly chosen and cells with aggregates were counted (Figure 12). For MG132 treatment we saw an increase in the percentage of cells with aggregates over time (from 38% to 64%, respectively, at 8h and 24h). In contrast, for untreated and FK866 treated cells this percentage is similar until 24h of treatment (around 30%). When we treated the cells with MG132 and FK866 simultaneously, the percentage of cells with aggregates is higher than the effect of each inhibitor alone at 8h (49%) and this percentage also increases until 24h of treatment that present identical values to MG132 treatment alone (64%). However, a quantitative analysis of a higher number of cells are needed to confirm these results. Other approaches could include the study of the number, size and quantification of the fluorescence intensity of the aggregates of each cell by each condition.

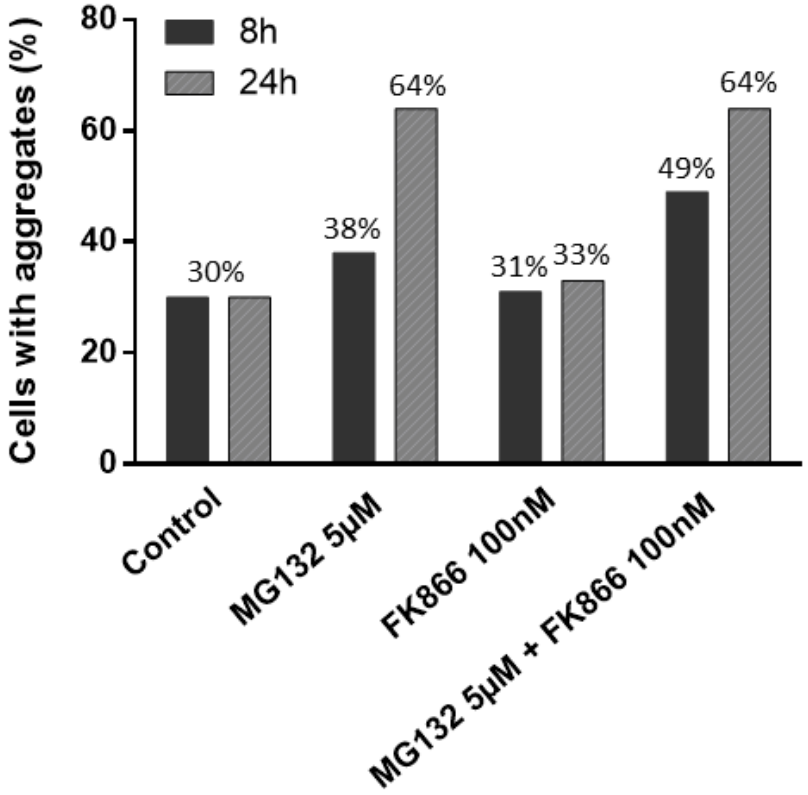

FIGURE 12. PERCENTAGE OF SH-SY5Y CELLS WITH AGGREGATES OVER TIME (8H AND 24H).

One hundred cells were randomly chosen and cells with aggregates were counted.

We expected to see a greater difference in the percentage of cells with aggregates at 8h between untreated and MG132 treated cells but the small differences observed are according to the MFI obtained by flow cytometry (Figure 10). Although MG132 does not increase cell death in SH-SY5Y cells nor compromises the cellular metabolic state until 16h of treatment, protein accumulation within cells over time was not surprising and would likely continue to increase with continued inhibition of the proteasome. These results are supported in the literature. In mouse neuroblastoma N2a cells that overexpressed TTC3 (human tetratricopeptide repeat domain 3), an increased number of cells formed TTC3 insoluble aggregates over time. The addition of proteasome inhibitor MG132 (10μM) resulted in more TTC3 aggregates in a short period of time (12h) [94].

In contrast with MG132, NAMPT inhibition appears not promote protein aggregate formation and this result is supported by the literature. In leukaemia cells, FK866 weakly induced ER stress through the increase in BIP, IRE1α and CHOP proteins, as well as increasing the accumulation of ubiquitinated proteins. However, when these cells are co-treated with FK866 and Cyclosporin-A (CsA, an Pgp – Glycerol-3-phosphate phosphatase - inhibitor) the effect of FK866 is exacerbated, resulting in higher increase in ER stress response proteins [95]. When we co-treated SH-SY5Y cells with MG132 and FK866 we saw an increase in protein aggregates compared to the effect of MG132 and FK866 alone. This result could be a consequence of the ER stress induced by both chemicals (Figure 11 G and 12).

3. *NAMPT* and *NAPRT* expression in SH-SY5Y cells

Next, we evaluated *NAMPT* and *NAPRT* expression by RT-PCR in SH-SY5Y cells treated with 5μM MG132, 100nM FK866 and 5μM MG132 plus 100nM FK866 during 8h and 24h. RNA was extracted as described in methods and used as a template for reverse transcription. An example of the results is shown in Figure 13. The size of the amplified products is 572bp, 454bp and 374bp for *GAPDH*, *NAMPT* and *NAPRT*, respectively. *NAMPT* appears to be less expressed than *NAPRT* in most treatments, however, both genes are expressed in low amounts when compared to *GAPDH* control. This was expected, as *NAMPT* and *NAPRT* gene are have weaker expression in the brain [36, 51]. *NAPRT* expression seems to be identical or slightly increased with all treatments. In contrast, *NAMPT* expression changes between conditions. Cells treated with the proteasome inhibitor MG132 present a gradual decrease in *NAMPT* expression until 24h of treatment, while the NAMPT inhibitor FK866 promotes a decrease in *NAMPT* expression at 8h and a pronounced increase at 24h. Treatment with both inhibitors show a similar expression pattern than MG132 treatment alone.

These results suggest that *NAMPT* expression is more sensitive to these conditions and *NAPRT* expression could sustain NAD levels under stress.

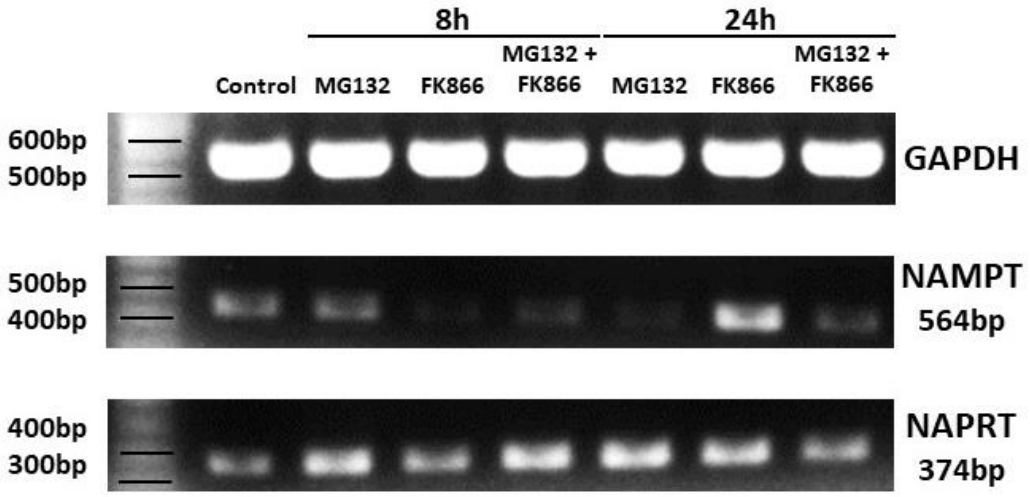

FIGURE 13. *NAMPT* AND *NAPRT* EXPRESSION IN SH-SY5Y CELLS.

RT-PCR analysis from SH-SY5Y cells treated with 5µM MG132, 100nM FK866 and 5µM MG132 plus 100nM FK866 for 8h and 24h. *GAPDH* is included as a control.

Indeed, in cultured primary muscle cells, NAD depletion triggered by FK866 resulted in increased expression of *NAMPT* and *NMRK2* [78]. It has been shown that CLOCK:BMAL1 complex binds to the promoter and to the first intron of *NAMPT* gene to upregulate its transcription [49, 51]. In our experiments, increase in *NAMPT* expression at 24h in cells treated with FK866 could be explained by this mechanism. An early decrease in *NAMPT* expression as observed at 8h of exposure, would result in NAD depletion, triggering the clock machinery that promotes *NAMPT* expression to restore NAD levels. This is also consistent with our results of the metabolic state of cells (Figure 9).

In cells treated with MG132, *NAMPT* expression decreases over time, suggesting that the feedback that induces *NAMPT* transcription is dependent of low NAD levels that are not attained in this condition. When treated with both compounds we observed a decrease in *NAMPT* expression over time also, indicating that the mechanism to promote *NAMPT* expression is also dependent of a functional proteasome (Figure 13).

For *NAPRT* expression, we observed a slight increase over time. In some gastric cancer cell lines, *NAPRT* expression is enough to maintain NAD levels in the presence of 20nM FK866 for 40h [36, 92]. We used a higher concentration (100nM), thus, in the presence of NAMPT inhibition, *NAPRT* can be overexpressed over time to compensate the induced stress (Figure 13). Taken together, these results suggest that NAMPT inhibition and NAD depletion are both required to induce *NAMPT*

transcription in SH-SY5Y cells while proteasome inhibition and normal NAD levels do not trigger this mechanism. To confirm the results, real time qPCR analysis should be performed to quantify *NAMPT* and *NAPRT* expression, as well as NMNATs and other NAD biosynthetic enzymes in our experimental conditions.

In Figure 14, we present a model that could explain *NAMPT* expression results, under the tested conditions for 24h, and describe how NAD levels regulate *NAMPT* transcription. In normal conditions, SH-SY5Y cells produce NAD in the cytoplasm, nucleus and mitochondria. NAD produced within the nucleus can be used by SIRT1, together with the CLOCK:BMAL1 complex, to promote *NAMPT* expression in response to mechanical and inflammatory signals. Thus, increasing *NAMPT* expression increases NAD levels and improves SIRT1 activity (Figure 14 A). However, when these cells are under stress conditions such as proteasome inhibition with MG132, *NAMPT* expression is repressed. NAD depletion may occur but not to critical levels and therefore, SIRT1 is not activated to bind to clock machinery and to induce *NAMPT* transcription (Figure 14 B). When SH-SY5Y cells are treated with the NAMPT inhibitor FK866, *NAMPT* expression is activated, as NAD levels decrease. This decrease and a functional proteasome stimulate *NAMPT* transcription through SIRT1 activation to restore NAD levels within the cell (Figure 14 C).

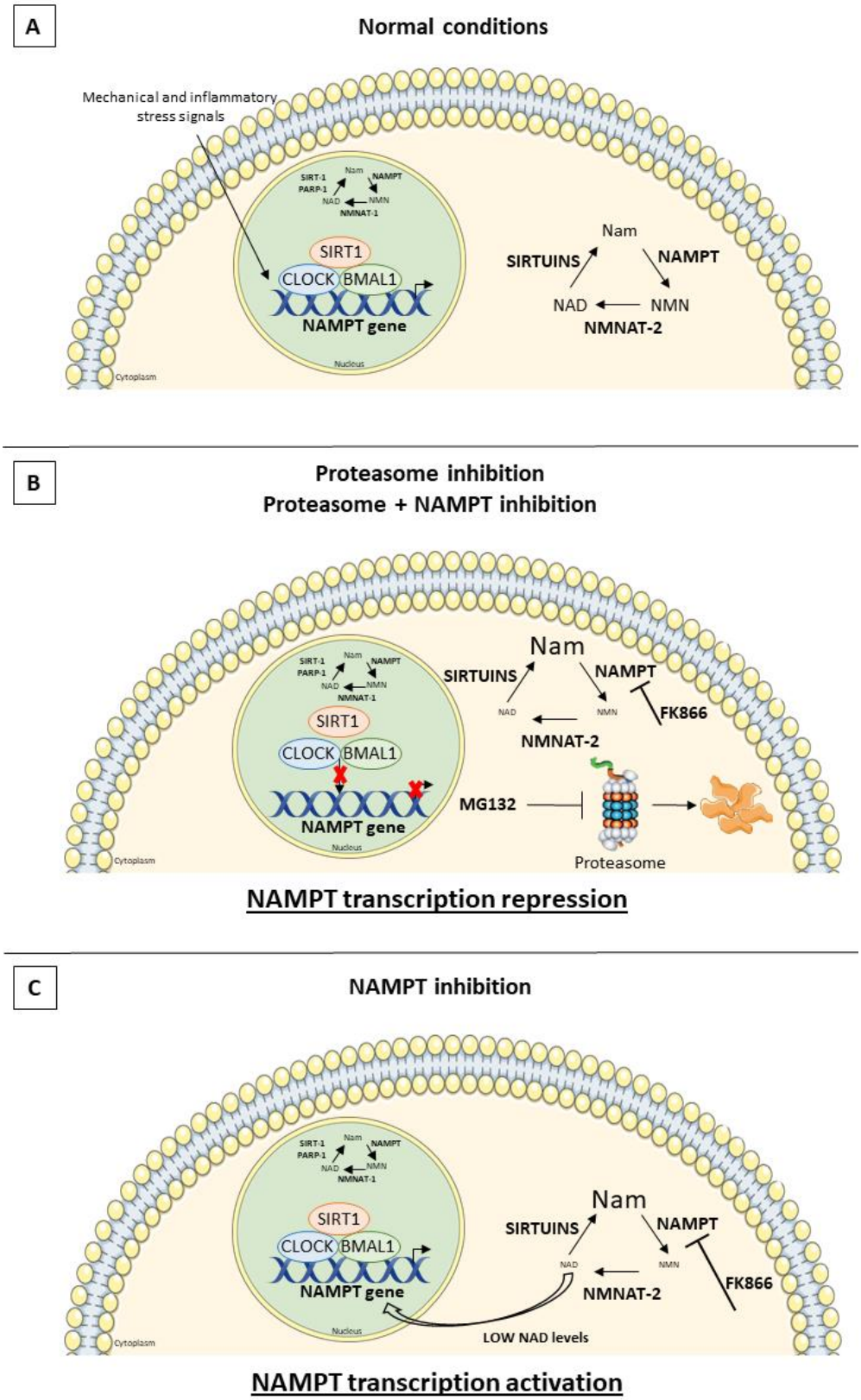

FIGURE 14. PROPOSED MODEL FOR *NAMPT* EXPRESSION UNDER STRESS CONDITIONS AFTER 24H.

A) Normal conditions, **B)** Treatment with the proteasome inhibitor MG132 **C)** Treatment with the NAMPT inhibitor FK866.

4. The effect of NAD and its precursors in protein aggregation in SH-SY5Y cells

We have supplemented the cells with NAD and its precursor nicotinamide mononucleotide (NMN) to evaluate the effect of these compounds in protein aggregation by flow cytometry. First, we analysed cell viability and for that SH-SY5Y cells were treated with MG132, FK866 and both chemicals simultaneously with 10mM NAD or 1mM NMN for 24h. After treatments, cells were immediately stained with 5µL propidium iodide and the results are presented in Figure 16. In the treatments with MG132 cell viability was not altered (red and blue lines are overlapped with the control line, black), and the number of viable (left peak) and dead (right peak) cells in these conditions are very similar as the lines almost overlap. In FK866-treated cells NAD does not alter viability (green and black line are overlapped), while in cells treated with NMN the viable cells (left green peak) present a shift with higher fluorescence intensity compared to control cells, however, the number of dead cells in untreated and NMN-treated cells is similar (right green and black lines are overlapped).

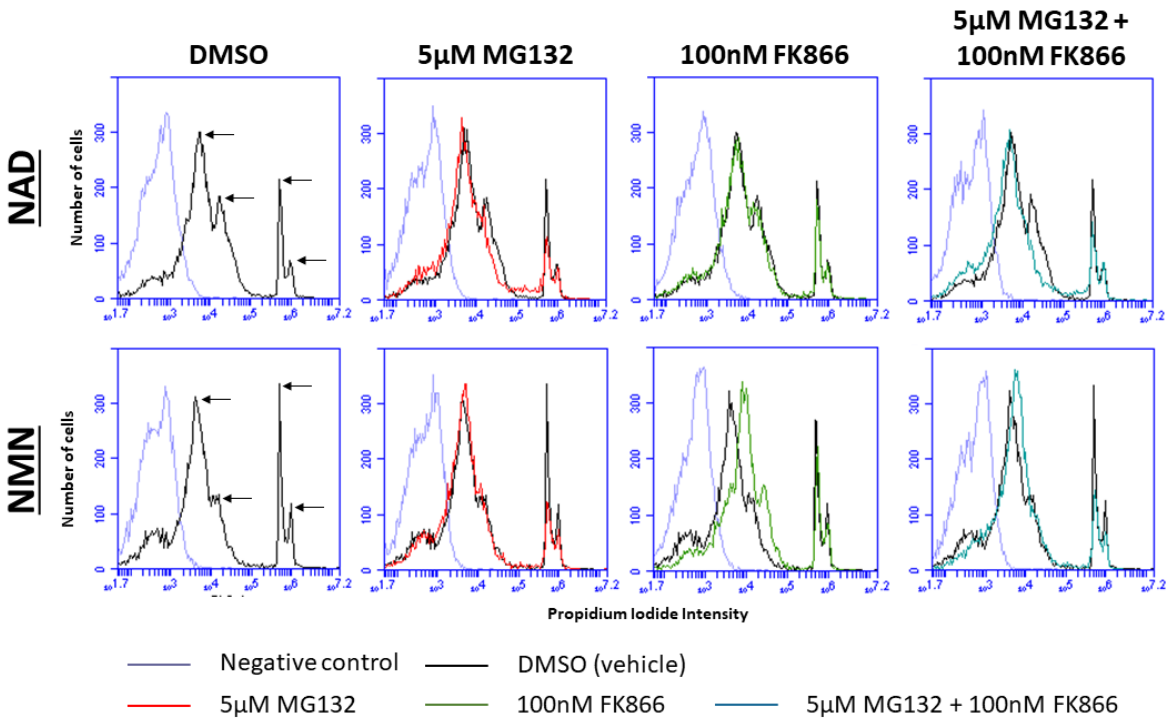

FIGURE 15. EFFECT OF NAD AND ITS PRECURSOR NMN IN SH-SY5Y CELL VIABILITY BY FLOW CYTOMETRY.

Representative histograms of Propidium Iodide fluorescence intensity measured by flow cytometry in cells treated with 5µM MG132, 100nM FK866 and 5µM MG132 plus 100nM FK866 simultaneously with 10mM NAD or 1mM NMN for 24h. The left peak in all graphs represents viable cells and the right peak represents dead cells with a total of 10.000 cells. Arrows represent different heterogeneous populations.

We also observed that viable and dead cells in all conditions present two peaks (represented by arrows), one with higher fluorescence intensity than the other, indicating that cells under NAD or NMN supplementation present heterogeneous populations (Figure 16). This could indicate that the cells do not respond in the same way or at the same time to precursors addition, resulting in different incorporation of PI amounts that is reflected in fluorescence intensity. To differentiate these populations, we could use Annexin V/Propidium Iodide, as previously suggested. Cell metabolic state was also evaluated using the resazurin assay and the metabolic state is not altered after 24h of exposure in all conditions (data not shown).

Overall, our results showed that nicotinamide mononucleotide addition has different effects than NAD addition in SH-SY5Y cells. The fact of NMN shifts the viable state in SH-SY5Y cells in the presence of the NAMPT inhibitor FK866 is surprising as NMN supplementation appears to be protective in aging and associated pathologies [8]. In the literature, supplementation with 15mM NAD for 24h in neuronal cultures ameliorates apoptotic neuronal death and inhibits the mitochondrial fragmentation after glutamate excitotoxicity [96]. Thus, our NAD results in cell viability are in agreement with previous findings.

Then, we evaluated the effect of NAD and NMN in protein aggregation by flow cytometry. For that, we treated SH-SY5Y cells as above. After treatments cells were fixed, permeabilized and stained with ProteoStat®. As well as in chapter 2, we used a fluorescence control to exclude autofluorescence and fluorescence intensity was measured in the FL3 channel. Viable cells were gated (P1 gate) according the Figure 10 A, while dead cells were excluded.

Representative histograms from flow cytometry results are presented in Figure 17. MG132-treated cells supplemented with NAD or NMN for 24h are similar, with higher fluorescence intensity than control cells that indicates more protein aggregates than controls but similar amounts between treatments. Surprisingly, FK866-treated cells supplemented with NMN present higher fluorescence intensity than FK866-treated cells supplemented with NAD, indicating that NMN has a role in protein aggregation under this condition. The absence of protein aggregates in the presence of NAD was expected, as FK866-treated cells present low protein aggregation (see chapter 2). Finally, for the last condition, in cells treated with both proteasome and NAMPT inhibitors, the mean higher fluorescence intensity than untreated cells reflects higher amounts of protein aggregates, although less for NAD than for NMN.

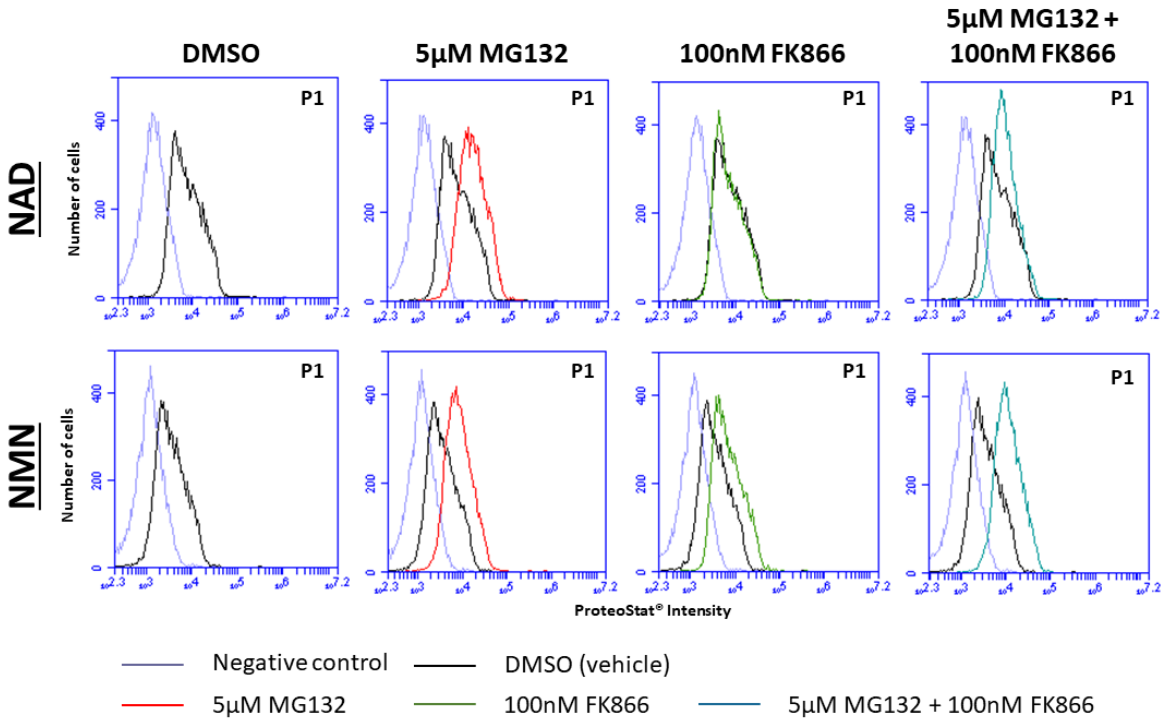

FIGURE 16. THE EFFECT OF NAD AND ITS PRECURSOR NMN IN PROTEIN AGGREGATION IN SH-SY5Y CELLS.

Representative histograms of ProteoStat® fluorescence intensity measured by flow cytometry in cells treated with inhibitors simultaneously with 10mM NAD or 1mM NMN for 24h. In each graph, only viable cells are represented with a total of 10.000 cells.

After analysing the effect of NAD and its precursor NMN in protein aggregation by flow cytometry, we used confocal microscopy to visualize the aggregates within the cells. SH-SY5Y cells were treated with the chemicals simultaneously with 10mM Nam and 1mM NMN for 24h. After treatments, cells were stained with ProteoStat® and DAPI to identify the aggregates (red) and the nucleus (blue), respectively.

Confocal microscopy results are shown in Figure 18. Control cells supplemented with Nam or NMN have low red fluorescence (Figure 18 E and I, respectively), as well as the untreated control cells (Figure 18 A), indicating that these cells contain identical and small amounts of protein aggregates. MG132-treated cells supplemented with both precursors, Nam and NMN, show high red fluorescence after 24h of exposure (Figure 18 F and J, respectively) and this fluorescence appears to be higher compared to the effect of MG132 alone (Figure 18 B), indicating that these cells present more protein aggregates. Cells treated with NAMPT inhibitor FK866 and simultaneously with its substrate Nam show low red fluorescence (Figure 18 G), indicating that these cells have less aggregation, as the effect of FK866 alone (Figure 18 C). This was expected once NAMPT is inhibited

to convert Nam into NMN. An identical effect was observed in cells treated with both MG132 and FK866, and Nam (Figure 18 H), which was not expected, as without Nam, the treatment with MG132 and FK866 shows high protein aggregation after 24h of exposure (Figure 11 G). NMN addition in FK866 treated cells and in cells treated with both chemicals, MG132 and FK866, promotes higher levels of red fluorescence compared to the effect of inhibitors alone (Figure 18 L and M, respectively), indicating that these cells have more amounts of protein aggregates. These results indicate that in SH-SY5Y cells, treatment with the NAMPT substrate Nam induces protein aggregate formation in cells with impaired proteasome function, while NMNAT-2 substrate NMN induces protein aggregation under all tested conditions.

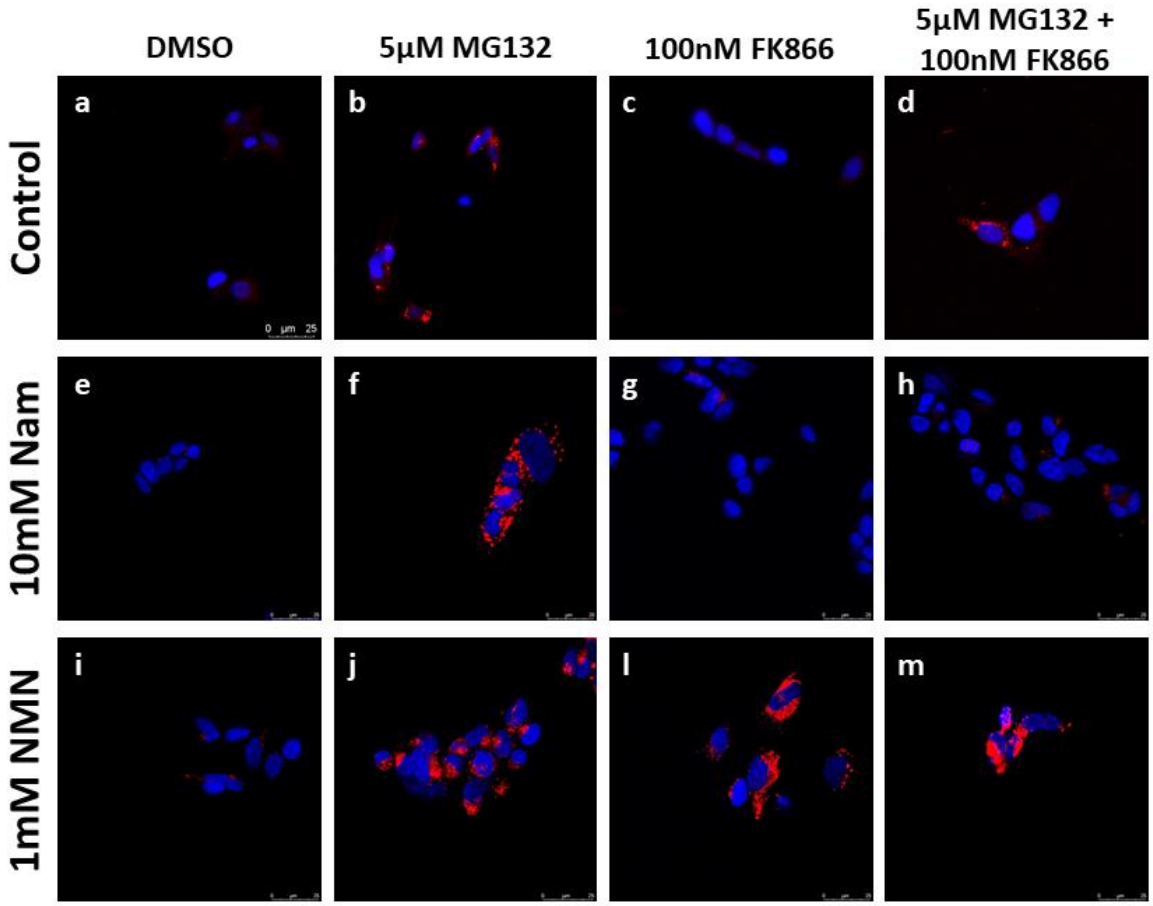

FIGURE 17. EFFECT OF NAD PRECURSORS IN PROTEIN AGGREGATION IN SH-SY5Y CELLS.

REPRESENTATIVE CONFOCAL IMAGES OF UNTREATED CELLS AND TREATED CELLS WITH 5µM MG132, 100NM FK866 AND 5µM MG132 PLUS 100NM FK866, SIMULTANEOUSLY, WITH 10MM NAM OR 1MM NMN FOR 24H. SCALE BAR REPRESENTS 25µM.

The model of Figure 15 represents the protein aggregation results. In normal conditions, NAMPT and NMNAT-2 act as NAD biosynthetic enzymes (Figure 15 A). When cells are exposed to proteasome inhibitor MG132, proteins are not degraded and accumulate within the cells (Figure 15

B). In contrast, induced NAD depletion through NAMPT inhibition reduces the availability of NMNAT-2 substrate, NMN. This could shift NMNAT-2 activity from NAD synthesis to act as a chaperone, as the protein has foldase or holdase activity, to clear or prevent the formation of aggregates. The aggregates that are formed rely on the proteasome system that is functional to degrade them (Figure 15 C). With both chemicals, NMN production is reduced through NAMPT inhibition that allows NMNAT-2 to act as chaperone, however, as the proteasome is also inhibited the protein aggregates that escaped from chaperone activity are not degraded and accumulate within the cells (Figure 15 D). This model supports the interplay between NAD metabolism and clearance of protein aggregates, that is supported by the literature [81-83].

According to our model, the effect of Nam in MG132 treated cells (Figure 18 F) could be a consequence of NMNAT-2 activity as NAD synthase instead of chaperone. In the presence of FK866, Nam appears to protect against protein aggregate formation (Figure 18 G), as NMNAT-2 has less substrate available. NAMPT inhibition results in no conversion of Nam into NMN and, therefore, NMNAT-2 shifts activity and acts as a chaperone. The idea that Nam addition has a beneficial effect is supported by the literature. Hepatocyte supplementation with 1mM of nicotinamide for 16h reduced the number of PI-positive cells (dead cells) and protected against palmitate-induced hepatotoxicity, representing a therapeutic choice for NAFLD [65]. In contrast, high concentrations of Nam have been used as a SIRT1 inhibitor in yeast and in human HepG2 cells, and this could lead to protein aggregate formation [97, 98]. FK866 is a non-competitive NAMPT inhibitor and, therefore, Nam is not accumulated within the cells preventing SIRT-1 inhibition, that is important to regulate *NAMPT* expression (Figure 13).

NMN result is surprising, as in the literature, NMN supplementation improves healthspan. In fact, pre-treatment of neurons with either levels of NAD in cell culture, or precursors such as nicotinamide mononucleotide, protects against axonal degeneration [99]. Moreover, NMN treatment rescues age-associated susceptibility to AKI (Acute Kidney Injury) in a SIRT1-dependent manner after 24h of exposure [100]. Our result is puzzling, as we saw protein aggregate formation in the presence of NMN supplementation. This could be caused by the displacement of NMNAT-2 to produce NAD instead acting as a chaperone (Figure 15), or the result may be attenuated with longer exposures. More studies are needed, such as NMNAT-2 protein expression levels measurements by Western Blot and co-localization with aggregates in microscopy experiments.

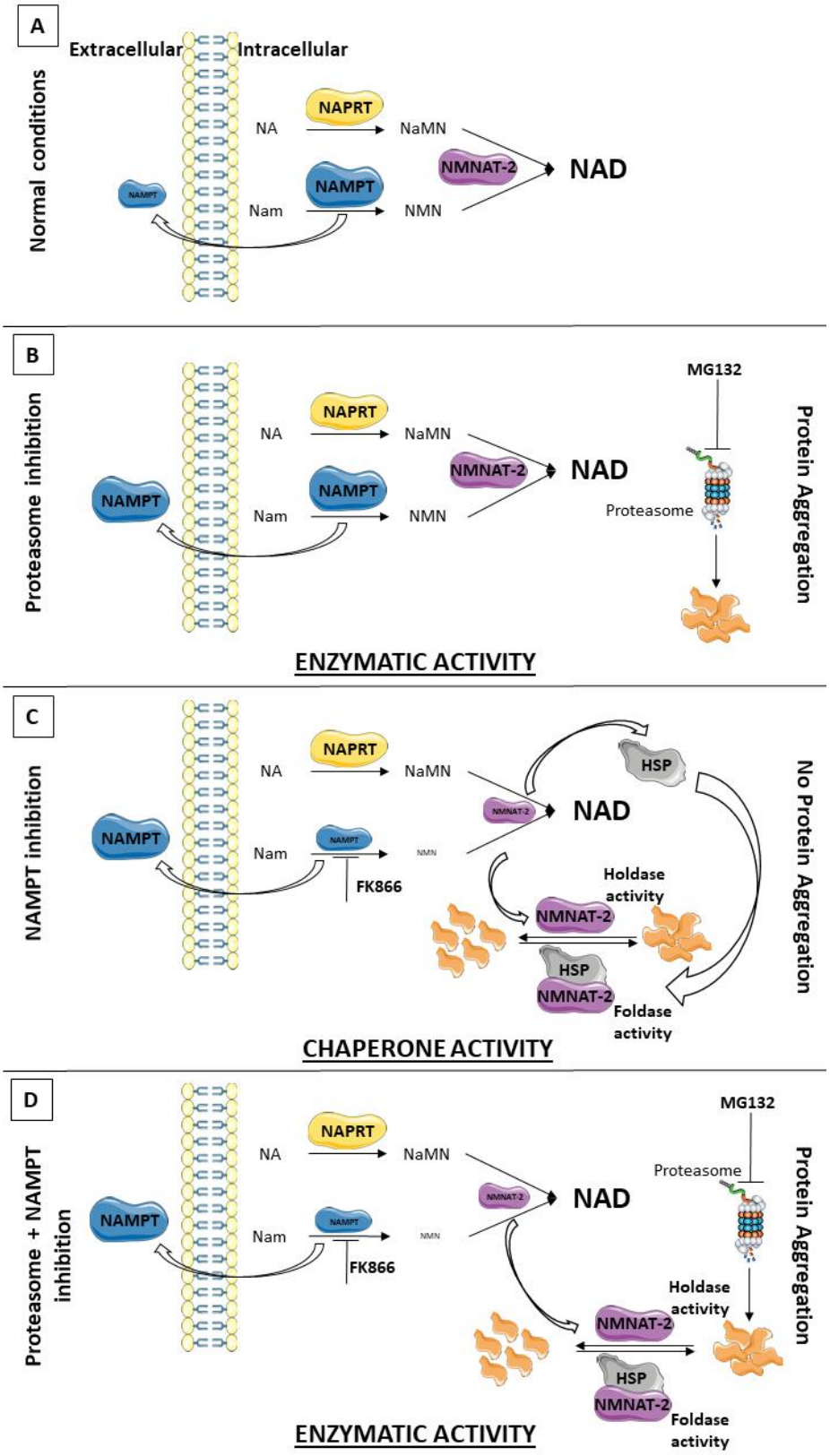

FIGURE 18. PROPOSED MODEL FOR NMNAT-2 ROLE IN PROTEIN AGGREGATION AFTER 24H.

A) Normal conditions, **B)** Proteasome inhibition with MG132, **C)** NAMPT inhibition with FK866 and **D)** Proteasome inhibition with MG132 plus NAMPT inhibition with FK866.

The protective effect of NAD was expected and supported by the literature. NAD supplementation appears to improve mice healthspan and prevent aggregate formation. Under NO-induced stress conditions, GAPDH and Siah Protein Enhances Life (GOSPEL) form amyloid-like aggregates that promote cell death. It has been described the potential of NAD to inhibit GAPDH-GOSPEL interaction by the covalent attachment of NAD to GAPDH active site, becoming permanently inactivated and preventing the formation of GAPDH aggregates [101]. Thus, according to our model (Figure 15), NAD addition could prevent protein aggregate formation and as the NAD pool was restored, allows NMNAT-2 to act as a chaperone.

CONCLUSION AND FUTURE PERSPECTIVES

Proteostasis is influenced by a continuous flow of misfolded or truncated proteins generated in gene expression and protein folding, that accumulate over time. Protein aggregation is associated with aging and with aging-related diseases, as well as NAD depletion. NAD replenishment appears to improve healthspan, but the exact molecular mechanisms responsible for their beneficial effect are not yet understood. To identify the interplay between NAD metabolism and protein aggregation we used SH-SY5Y cells as a model, and we evaluated cell death, cell metabolic state, protein aggregation and the expression of NAD biosynthetic enzymes in response to MG132, FK866, NAD and its precursors. We observed that MG132 and FK866 do not alter cell death in contrast with the metabolic state that is altered with the chemical treatments (Figure 7 and 9, respectively). We also showed that MG132 promotes protein aggregation in SH-SY5Y cells in contrast with FK866 (Figure 10 and 11). This lack of protein aggregation may be due to the action of NMNAT-2 that is recruited to act as chaperone for clearance and preventing the aggregates formation (Figure 16). We also propose that under these stress conditions, *NAPRT*, is overexpressed to restore NAD levels after 24h of exposure (Figure 13), while NAMPT inhibition promotes its transcription (Figure 14). In what concerns the supplementation experiments, we observed that NAD appears to prevent or eliminate protein aggregation in SH-SY5Y cells while NMN supplementation is cytotoxic for the same cells (Figure 17 and 18).

More experiments are needed to validate our hypothesis, such as: early and late apoptosis differentiation, for example using Annexin V / Propidium Iodide by flow cytometry; NAD levels measurements (NAD/NADH and NAD(P)/NAD(P)H, using commercial kits or mass spectrometry; number, size and type of protein aggregates identification by confocal microscopy and immunocytochemical analysis and co-localization experiments; supplementation with other NAD precursors, namely NR and Trp; quantify the RNA and protein expression levels of NAD biosynthetic enzymes using qRT-PCR and Western Blot, respectively; perform similar experiments in additional aging and aggregation models, such as cells with high passages, exposure to different chemical compounds and use different cell lines and models of proteinopathies.

Taken together, the results indicate that protein aggregate clearance through NAMPT inhibition and/or NAD supplementation, could be used as novel therapeutic strategies to improve healthspan in neurodegenerative diseases.

REFERENCES

References

1. Guo J, et al. *Identification of novel resistance mechanisms to NAMPT inhibition via the de novo NAD+ biosynthesis pathway and NAMPT mutation.* Biochemical and Biophysical Research Communications, 2017. **491**(3): p. 681-686.
2. Katsyuba E and Auwerx J. *Modulating NAD⁺ metabolism, from bench to bedside.* The EMBO journal, 2017. **36**(18): p. 2670-2683.
3. Imai S and Guarente L. *NAD⁺ and sirtuins in aging and disease.* Trends in cell biology, 2014. **24**(8): p. 464-471.
4. Chini CCS, Tarragó MG and Chini EN. *NAD and the aging process: Role in life, death and everything in between.* Molecular and cellular endocrinology, 2017. **455**: p. 62-74.
5. Ussher JR, et al. *Pyridine nucleotide regulation of cardiac intermediary metabolism.* Circulation Research, 2012. **111**(5): p. 628-41.
6. Xu R, et al. *Inhibition of NAMPT decreases cell growth and enhances susceptibility to oxidative stress.* Oncology Reports, 2017(38): p. 1767-1773.
7. Xiao W, et al. *NAD(H) and NADP(H) Redox Couples and Cellular Energy Metabolism.* Antioxidants Redox Signaling, 2018. **28**(3): p. 251-272.
8. Verdin E. *NAD⁺ in aging, metabolism, and neurodegeneration.* Science, 2015. **350**(6265): p. 1208-1213.
9. Wang P, et al. *NAMPT and NAMPT-controlled NAD Metabolism in Vascular Repair.* ournal of Cardiovascular Pharmacology, 2016. **67**(6): p. 474–481.
10. Grahnert A, et al. *NAD⁺: A modulator of immune functions.* Innate Immunity, 2011. **17**(2): p. 212-233.
11. Belenky P, Bogan KL, and Brenner C. *NAD⁺ metabolism in health and disease.* Trends in Biochemical Sciences, 2007. **32**(1): p. 12-19.
12. Chang HC and Guarente L. *SIRT1 and other sirtuins in Metabolism.* Trends in endocrinology and metabolism. 2014. **25**(3): p. 138-145.
13. Gibson BA and Kraus WL. *New insights into the molecular and cellular functions of poly(ADP-ribose) and PARPs.* Nat Rev Mol Cell Biol, 2012. **13**(7): p. 411-424.
14. Chini EN. *CD38 as a Regulator of Cellular NAD: A Novel Potential Pharmacological Target for Metabolic Conditions.* Current pharmaceutical design, 2009. **15**(1): p. 57-63.
15. Nady Braidy JB, et al. *Role of NAD and related Precursors as Therapeutic Targets for Age-related Degenerative Diseases: Rationale, Biochemistry, Pharmacokinetics, and Outcomes.* Antioxidants and Redox Signaling, 2018.
16. Essuman K, et al. *The SARM1 Toll/Interleukin-1 Receptor Domain Possesses Intrinsic NAD+ Cleavage Activity that Promotes Pathological Axonal Degeneration.* Neuron, 2017. **93**(6): p. 1334-1343.
17. Essuman K, et al. *TIR Domain Proteins Are an Ancient Family of NAD⁺-Consuming Enzymes.* Current Biology, 2018. **28**(3): p. 421-430.e4.
18. Summers DW, et al. *SARM1-specific motifs in the TIR domain enable NAD⁺ loss and regulate injury-induced SARM1 activation.* Proceedings of the National Academy of Sciences of the United States of America, 2016. **113**(41): p. E6271-E6280.
19. Goldner R and Yaron A. *TIR Axons Apart: Unpredicted NADase Controls Axonal Degeneration.* Neuron, 2017. **93**(6): p. 1239-1241.
20. Li J, et al. *A conserved NAD⁺ binding pocket that regulates protein-protein interactions during aging.* Science, 2017. **355**(6331): p. 1312.
21. Ternes CM and Schönknecht G. *Gene Transfers Shaped the Evolution of De Novo NAD⁺ Biosynthesis in Eukaryotes.* Genome Biology and Evolution, 2014. **6**(9): p. 2335-2349.

22. Yamaguchi S and Yoshino J. *Adipose Tissue NAD$^+$ Biology in Obesity and Insulin Resistance: From Mechanism to Therapy.* BioEssays: news and reviews in molecular, cellular and developmental biology, 2017. **39**(5).
23. Rajman L, Chwalek K and Sinclair DA. *Therapeutic Potential of NAD-Boosting Molecules: The In Vivo Evidence.* Cell metabolism, 2018. **27**(3): p. 529-547.
24. Stromsdorfer KL, et al. *NAMPT-mediated NAD$^+$ biosynthesis in adipocytes regulates adipose tissue function and multi-organ insulin sensitivity in mice.* Cell reports, 2016. **16**(7): p. 1851-1860.
25. Revollo JR, Grimm AA and Imai S. *The NAD Biosynthesis Pathway Mediated by Nicotinamide Phosphoribosyltransferase Regulates Sir2 Activity in Mammalian Cells.* The Journal of Biological Chemistry, 2004. **279**(49): p. 50754-50763.
26. Imai S. *Nicotinamide phosphoribosyltransferase (Nampt): A link between NAD biology, metabolism, and diseases.* Current pharmaceutical design, 2009. **15**(1): p. 20-28.
27. Garrido A and Djouder N. *NAD$^+$ Deficits in Age-Related Diseases and Cancer.* Trends in Cancer, 2017. **3**(8): p. 593-610.
28. de Figueiredo LF, Gossmann TI, et al. *Pathway analysis of NAD+ metabolism.* Biochemical Journal, 2011. **439**(2): p. 341–348.
29. Shi H, et al. *NAD Deficiency, Congenital Malformations, and Niacin Supplementation.* The New England Journal of Medicine, 2017. **377**(6): p. 544-552.
30. Guo J, et al. *Identification of novel resistance mechanisms to NAMPT inhibition via the de novo NAD+ biosynthesis pathway and NAMPT mutation.* Biochemical and Biophysical Research Communications, 2017. **491**(3): p. 681-686.
31. Liu L, et al. *Quantitative Analysis of NAD Synthesis-Breakdown Fluxes.* Cell Metabolism, 2018. **27**(5): p. 1067-1080.
32. Nikiforov A, et al. *Pathways and Subcellular Compartmentation of NAD Biosynthesis in Human Cells: from entry of extracellular precursores to mitochondrial NAD generation.* The Journal of Biological Chemistry, 2011. **286**(24): p. 21767-21778.
33. Poljsak B. *NAMPT-Mediated NAD Biosynthesis as the Internal Timing Mechanism: In NAD$^+$ World, Time Is Running in Its Own Way.* Rejuvenation Research, 2017. p. 51.
34. Bieganowski P and Brenner C. *Discoveries of Nicotinamide Riboside as a Nutrient and Conserved NRK Genes Establish a Preiss-Handler Independent Route to NAD$^+$ in Fungi and Humans.* Cell, 2004. **117**(4): p. 495-502.
35. Garten A, et al. *Physiological and pathophysiological roles of NAMPT and NAD metabolism.* Nature Reviews Endocrinology, 2015. **11**: p. 535-546.
36. Duarte-Pereira S, et al. *Extensive regulation of nicotinate phosphoribosyltransferase (NAPRT) expression in human tissues and tumors.* Oncotarget, 2016. **7**(2): p. 1973-1983.
37. Samal B, et al. *Cloning and characterization of the cDNA encoding a novel human pre-B-cell colony-enhancing factor.* Molecular and Cellular Biology, 1994. **14**(2): p. 1431-1437.
38. Imai S. *The NAD World: A new systemic regulatory network for metabolism and aging – Sirt1, systemic NAD biosynthesis, and their importance.* Cell biochemistry and Biophysics, 2009. **53**(2): p. 65-74.
39. Martin PR, et al. *Identification of a Plasmid-Encoded Gene from Haemophilus ducreyi Which Confers NAD Independence.* Journal of Bacteriology, 2001. **183**(4): p. 1168-1174.
40. Sampath D, et al. *Inhibition of nicotinamide phosphoribosyltransferase (NAMPT) as a therapeutic strategy in cancer.* Pharmacology and Therapeutics, 2015. **151**: p. 16-31.
41. Chen X, et al. *The Role of Nicotinamide Phosphoribosyltransferase in Cerebral Ischemia.* Current topics in medicinal chemistry, 2015. **15**(21): p. 2211-2221.
42. Garten A, et al. *Nicotinamide phosphoribosyltransferase (NAMPT/PBEF/visfatin) is constitutively released from human hepatocytes.* Biochemical and Biophysical Research Communications, 2010. **391**(1): p. 376-381.

43. Grolla AA, et al. *Extracellular nicotinamide phosphoribosyltransferase, a new cancer metabokine.* British Journal of Pharmacology, 2016. **173**(14): p. 2182-2194.
44. Imai S and Guarente L. *It takes two to tango: NAD$^+$ and sirtuins in aging/longevity control.* NPJ Aging and Mechanisms of Disease, 2016. **2**: p. 16017.
45. Imai S. *Dissecting Systemic Control of Metabolism and Aging in the NAD World: The Importance of SIRT1 and NAMPT-mediated NAD Biosynthesis.* FEBS letters, 2011. **585**(11): p. 1657-1662.
46. Shu-Na Wang, et al. *Targeting Nicotinamide Phosphoribosyltransferase as a Potential Therapeutic Strategy to Restore Adult Neurogenesis.* CNS Neuroscience and Therapeutics, 2016. **22**(6): p. 431-9.
47. Rehan L, et al. *SIRT1 and NAD as regulators of ageing.* Life Sciences, 2014. **105**(1): p. 1-6.
48. Nakahata Y and Bessho Y. *The Circadian NAD$^+$ Metabolism: Impact on Chromatin Remodeling and Aging.* BioMed Research International, 2016. **2016**: p. 7.
49. Ramsey KM, et al. *Circadian Clock Feedback Cycle Through NAMPT-Mediated NAD$^+$ Biosynthesis.* Science (New York, N.Y.), 2009. **324**(5927): p. 651-654.
50. Imai S. *The NAD World 2.0: the importance of the inter-tissue communication mediated by NAMPT/NAD$^+$/SIRT1 in mammalian aging and longevity control.* Systems Biology And Applications, 2016. **2**: p. 16018.
51. Imai S. *"Clocks" in the NAD World: NAD as a Metabolic Oscillator for the Regulation of Metabolism and Aging.* Biochimica Biophys Acta, 2010. **1804**(8): p. 1584-1590.
52. Mouchiroud L, et al. *The NAD$^+$/sirtuin pathway modulates longevity through activation of mitochondrial UPR and FOXO signaling.* Cell, 2013. **154**(2): p. 430-441.
53. Mendelsohn AR and Larrick JW. *The NAD$^+$/PARP1/SIRT1 Axis in Aging.* Rejuvenation Research, 2017. **20**(3): p. 244-247.
54. Fu Xi, et al. *Endoplasmic reticulum proteins quality control and the unfolded protein response: The regulative mechanism of organisms against stress injuries.* BioFactors, 2014. **40**(6): p. 569-585.
55. Ni M and Lee AS. *ER chaperones in mammalian development and human diseases.* FEBS letters, 2007. **581**(19): p. 3641-3651.
56. Press M, et al. *Protein aggregates and proteostasis in aging: Amylin and β-cell function.* Mechanisms of Ageing and Development, 2018. **637**(18): p.30045-9.
57. Wang R, et al. *Immune regulation of the unfolded protein response at the mucosal barrier in viral infection.* Clinical and Translational Immunology, 2018. **7**(4): p. e1014.
58. Terakawa MS, et al. *Impact of membrane curvature on amyloid aggregation.* Biochimica et Biophysica Acta Biomembranes, 2018. **2736**(18): p. 30130-5.
59. Nillegoda NB, Wentink AS and Bukau B. *Protein Disaggregation in Multicellular Organisms.* Trends in Biochemical Sciences, 2018. **43**(4): p. 285-300.
60. Sigurdsson V and Miharada K. *Regulation of unfolded protein response in hematopoietic stem cells.* International Journal of Hematology, 2018.
61. Dobson CM. *Protein folding and misfolding.* Nature, 2003. **426**: p. 884-90.
62. Feldman DE and Frydman J. *Protein folding in vivo: the importance of molecular chaperones.* Current Opinion in Structural Biology, 2000. **10**(1): p. 26-33.
63. Tsakiri EN and Trougakos IP. *The Amazing Ubiquitin-Proteasome System: Structural Components and Implication in Aging*, in *International Review of Cell and Molecular Biology*, 2015. **314**: p. 171-237.
64. Su H and Wang X. *The ubiquitin-proteasome system in cardiac proteinopathy: a quality control perspective.* Cardiovascular research, 2010. **85**(2): p. 253-262.
65. Shen C, et al. *Nicotinamide protects hepatocytes against palmitate-induced lipotoxicity via SIRT1-dependent autophagy induction.* Nutrition research (New York, N.Y.), 2017. **40**: p. 40-47.

66. Kernan J, Bonacci T and Emanuele MJ. *Who guards the guardian? Mechanisms that restrain APC/C during the cell cycle.* Biochim Biophys Acta - Molecular Cell Research, 2018. **1865**(12): p. 1924-1933.
67. Kocaturk NM and Gozuacik D. *Crosstalk Between Mammalian Autophagy and the Ubiquitin-Proteasome System.* Frontiers in Cell and Developmental Biology, 2018. **6**(128).
68. Hetz C, Chevet E and Oakes SA. *Proteostasis control by the unfolded protein response.* Nature cell biology, 2015. **17**(7): p. 829-838.
69. Shaheen A. *Effect of the unfolded protein response on ER protein export: a potential new mechanism to relieve ER stress.* Cell Stress and Chaperones, 2018. **23**(8): p. 797-806.
70. Ri M. *Endoplasmic-reticulum stress pathway-associated mechanisms of action of proteasome inhibitors in multiple myeloma.* International Journal of Hematology, 2016. **104**(3): p. 273-280.
71. Shpilka T and Haynes CM. *The mitochondrial UPR: mechanisms, physiological functions and implications in ageing.* Nature Reviews Molecular Cell Biology, 2017. **19**: p. 109.
72. Tyedmer J, Mogk A and Bukau B. *Cellular strategies for controlling protein aggregation.* Nature Reviews Molecular Cell Biology, 2010. **11**: p. 777.
73. Martínez G, et al. *Endoplasmic reticulum proteostasis impairment in aging.* Aging Cell, 2017. **16**(4): p. 615-623.
74. Satoh A, Imai S and Guarente L. *The brain, sirtuins, and ageing.* Nature Reviews Neuroscience, 2017. **18**: p. 362.
75. Zhang M and Ying W. *NAD^+ Deficiency Is a Common Central Pathological Factor of a Number of Diseases and Aging: Mechanisms and Therapeutic Implications.* Antioxidants and Redox Signaling, 2018.
76. Fang EF, et al. *NAD^+ in Aging: Molecular Mechanisms and Translational Implications.* Trends in Molecular Medicine, 2017. **23**(10): p. 899-916.
77. Sultani G, et al. *NAD^+: A key metabolic regulator with great therapeutic potential.* Journal of Neuroendocrinology, 2017. **29**(10): p. e12508.
78. Fletcher RS, et al. *Nicotinamide riboside kinases display redundancy in mediating nicotinamide mononucleotide and nicotinamide riboside metabolism in skeletal muscle cells.* Molecular Metabolism, 2017. **6**(8): p. 819-832.
79. Johnson S and Imai S. *NAD^+ biosynthesis, aging, and disease.* F1000Research, 2018. **7**: p. 132-132.
80. Brazill JM, et al. *NMNAT: It's an NAD^+ synthase… It's a chaperone… It's a neuroprotector.* Current opinion in genetics & development, 2017. **44**: p. 156-162.
81. Lavado-Roldán A and Fernández-Chacón R. *Two for the Price of One: A Neuroprotective Chaperone Kit within NAD Synthase Protein NMNAT2.* PLOS Biology, 2016. **14**(7): p. e1002522.
82. Zhai RG, et al. *NAD synthase NMNAT acts as a chaperone to protect against neurodegeneration.* Nature, 2008. **452**(7189): p. 887-891.
83. Ocampo A, Liu J and Barrientos A. *NAD^+ salvage pathway proteins suppress proteotoxicity in yeast models of neurodegeneration by promoting the clearance of misfolded/oligomerized proteins.* Human molecular genetics, 2013. **22**(9): p. 1699-1708.
84. Knowles TPJ, Vendruscolo M and Dobson CM. *The amyloid state and its association with protein misfolding diseases.* Nature Reviews Molecular Cell Biology, 2014. **15**: p. 384.
85. Pietkiewicz S, Schmidt JH and Lavrik IN. *Quantification of apoptosis and necroptosis at the single cell level by a combination of Imaging Flow Cytometry with classical Annexin V/propidium iodide staining.* Journal of Immunological Methods, 2015. **423**: p. 99-103.
86. Walzl A, et al. *The Resazurin Reduction Assay Can Distinguish Cytotoxic from Cytostatic Compounds in Spheroid Screening Assays.* Journal of Biomolecular Screening, 2014. **19**(7): p. 1047-1059.

87. Koontz L. *Agarose Gel Electrophoresis*, in *Methods in Enzymology*, J. Lorsch, Editor. 2013, Academic Press. **529:** p. 35-45.
88. Han YH, et al. *"The effect of MG132, a proteasome inhibitor on HeLa cells in relation to cell growth, reactive oxygen species and GSH".* Oncology Reports 2009. **22**(1): p. 215-221.
89. Hasmann M and Schemainda I. *FK866, a Highly Specific Noncompetitive Inhibitor of Nicotinamide Phosphoribosyltransferase, Represents a Novel Mechanism for Induction of Tumor Cell Apoptosis.* Cancer Research, 2003. **63**(21): p. 7436-7442.
90. Kummrow A, et al. *Quantitative assessment of cell viability based on flow cytometry and microscopy.* Journal of Quantitative Cell Science, 2013. **83A**(2): p. 197-204.
91. Schuster S, et al. *FK866-induced NAMPT inhibition activates AMPK and downregulates mTOR signaling in hepatocarcinoma cells.* Biochemical and Biophysical Research Communications, 2015. **458**(2): p. 334-340.
92. Lee J, et al. *Selective Cytotoxicity of the NAMPT Inhibitor FK866 Toward Gastric Cancer Cells With Markers of the Epithelial-Mesenchymal Transition, Due to Loss of NAPRT.* Gastroenterology, 2018. **155**(3): p. 799-814.e13.
93. Ortiz-Lazareno PC, et al. *Sensitization of U937 leukemia cells to doxorubicin by the MG132 proteasome inhibitor induces an increase in apoptosis by suppressing NF-kappa B and mitochondrial membrane potential loss.* Cancer Cell International, 2014. **14**: p. 13-13.
94. Gong Y, et al. *Overexpressed TTC3 Protein Tends to be Cleaved into Fragments and Form Aggregates in the Nucleus.* NeuroMolecular Medicine, 2018.
95. Cagnetta A, et al. *APO866 Increases Antitumor Activity of Cyclosporin-A by Inducing Mitochondrial and Endoplasmic Reticulum Stress in Leukemia Cells.* Clinical Cancer Research, 2015. **21**(17): p. 3934.
96. Wang X, Li H and Ding S. *The effects of NAD^+ on apoptotic neuronal death and mitochondrial biogenesis and function after glutamate excitotoxicity.* International journal of molecular sciences, 2014. **15**(11): p. 20449-20468.
97. Bitterman KJ, et al. *Inhibition of Silencing and Accelerated Aging by Nicotinamide, a Putative Negative Regulator of Yeast Sir2 and Human SIRT1.* Journal of Biological Chemistry, 2002. **277**(47): p. 45099-45107.
98. Hou X, et al. *SIRT1 regulates hepatocyte lipid metabolism through activating AMP-activated protein kinase.* The Journal of biological chemistry, 2008. **283**(29): p. 20015-20026.
99. Cantó C, Menzies K and Auwerx J. *NAD^+ metabolism and the control of energy homeostasis - a balancing act between mitochondria and the nucleus.* Cell metabolism, 2015. **22**(1): p. 31-53.
100. Guan Y, et al. *Nicotinamide Mononucleotide, an NAD^+ Precursor, Rescues Age-Associated Susceptibility to AKI in a Sirtuin 1-Dependent Manner.* Journal of the American Society of Nephrology : JASN, 2017. **28**(8): p. 2337-2352.
101. González MC, et al. *Enhancement by GOSPEL protein of GAPDH aggregation induced by nitric oxide donor and its inhibition by NAD+.* FEBS Letters, 2016. **590**(14): p. 2210-2220.

ANNEXES

Annex 1

List of used materials in this study are described below.

Cell culture solutions

Minimum Essential Medium (MEM), Gibco

F12 Nutrient Mixture, Gibco

Sodium Bicarbonate ($NaHCO_3$), Sigma

Sodium Pyruvate, Sigma

Antibiotic-Antimycotic, 100x (AA´s), Gibco

L-Glutamine, 200mM, Gibco

Resazurin solution, Sigma

Fetal Bovine Serum (FBS), qualified, E.U.-approved, South America origin, Gibco

Trypsin-EDTA (0,05%), phenol red, Gibco

Phosphate Buffer Saline, pH 7,4, Gibco

Dimethyl sulfoxide (DMSO), Gibco

Markers and loading dyes

Sample Buffer, Laemmli 2xConcentrate, Sigma – S3401

NZYDNA Ladder V, NzyTech – MB06101

5x Nucleic Acid Sample Buffer, Bio-Rad - #1610767

GreenSafe Premium, NyzTech – MB13201

Kits

Proteostat® Aggresome Detection Kit, ENZ-51035-K100

Direct-zol™ RNA MiniPrep, Zymo Research - R2050

Tetro Cdna Synthesis Kit, Bioline - 65042

HotStarTaq® Master Mix Kit, QIAGEN – 203443

SuperScript® II Enzyme Reverse Transcriptase, Invitrogen - 18064014

Primers

Table 1. List of primers used in this study.

Gene	Strand	Primer Sequence	Amplicon size
GAPDH (human)	Forward	5' CCAGCCGAGCCACATCG 3'	572bp
	Reverse	5´ GGTCATGAGTCCTTCCACG 3'	
NAMPT (human)	Forward	5' CTC ATT TTT CTC CTT CCT CGC 3'	454bp
	Reverse	5' TCC TCT GGG AAT GAC AAA GC 3'	
NAPRT (human)	Forward	5´ TATGCCTTGGCTTTTCCCCG 3'	374bp
	Reverse	5´ GCCACCAGCTTATAGACGC 3'	

Chemicals

All chemicals were obtained from Sigma, except MG132 that was obtained from the Proteostat® Aggresome Detection Kit, ENZO.

Chemical	Final concentration	Stock solution
MG132	5µM	Dilute 5mg of MG132 in 12µL of DMSO (10mM)
FK866	100nM	Dilute 5mg of FK866 in 1.168mL of DMSO (10mM)
NAD	10mM	Dilute 6.6343g of NAD in 1mL of ultra-pure water (1M)
Nicotinamide	10mM	Dilute 0.122g of Nam in 1mL of ultra-pure water (1M)
Nicotinamide Mononucleotide	1mM	Dilute 0.0235g of NMN in 70.5µL of ultra-pure water (1M)

Reagents

Mounting Medium for Fluorescence with DAPI, VECTOR Laboratories

TRIZOL, Invitrogen™

DNase I, Invitrogen™ (6U/µL)

-Add 5µL DNase I to 75µL Digestion Buffer

Agarose, NzyTech

Solutions and Buffers

Recipes of the used solutions and buffers in this study are described below. All buffers and solutions were prepared with demineralized water and if necessary, filter sterilized or autoclaved for long-term storage.

a. SDS - Polyacrylamide Gel Electrophoresis and Western Blotting

i. 2xLaemmli Buffer, pH 6.8

4% SDS

20% Glycerol

10% β-Mercapthanol

0,004% Bromophenol Blue

0,125M Tris-HCl

ii. Stacking gel Buffer

0,5M Tris-HCl, pH 6,8

iii. Resolving gel Buffer

1,5M Tris-HCl, pH 8,0

iv. Gel Running Buffer

250mM Tris

1,9M Glycine

1% SDS

v. Blotting Buffer (TGM – Tris-Cl, Glycine and Methanol)

700mL Ultrapure water

200mL Methanol

100mL Tris/Gly/SDS 10x

2mL 20% SDS

vi. 10x Tris Buffered Saline (TBS), pH 7.4

20mM Tris

0,9% NaCl

vii. Tris Buffered Saline – Tween20 (TBS-T) Buffer

20mM Tris

0,9% NaCl

0,1% Tween20

viii. Enhanced Chemiluminescence (ECL) Solution

Solution A: Luminol Solution

Solution B: Peroxidase

ix. Ponceau S

0.1% Ponceau S

5% Acetic Acid

x. Blocking Solution (TBS-T 5% low-fat milk)

20mM Tris

0,9% NaCl

0,1% Tween20

5% low-fat milk

xi. 10% Ammonium Persulfate (APS)

Dilute 100mg of APS in 1mL of ddH_2O

xii. Antibodies Solution

20mM Tris

0,9% NaCl

0,1% Tween20

1% low-fat milk

b. Agarose Gel Electrophoresis

i. 5x Nucleic Acid Sample Buffer

50Mm Tris-HCl, pH 8.0

25% Glycerol

5mM EDTA

0,2% Bromophenol Blue

0,2% Xylene Cyanole

ii. 50x Tris-Acetate-EDTA Buffer (TAE)

To 600mL of ddH_2O add:

- 242g Tris Base
- 57,1mL Glacial Acetic Acid
- 100mL 0,5M EDTA (pH 8,0)

iii. 1% Agarose Gel

Dilute 1g of agarose in 100mL of 1xTAE

c. Other solutions

i. 1xPhosphate Buffer Saline (PBS)

8mM Sodium Phosphate

2mM Potassium Phosphate

140mM Sodium Chloride

0,27mM Potassium Chloride

ii. 1xAssay Buffer

Each mL of Assay Buffer 10x was diluted in 9mL of deionized water

iii. 4%Paraformaldehyde (PFA)

Dilute 0,4g of paraformaldehyde in 10mL of 1xAssay Buffer

iv. 0,5%Triton-X100 WITH 3mM EDTA

Add 50µL of TRITON X-100 and 60µL of 0,5M EDTA in 9,89mL of 1xAssay Buffer

v. 10%Resazurin

Dilute 0,1mg in 1mL of 1xPBS

vi. 1%Bovine Serum Albumin (BSA)

Dilute 2%BSA in 1xPBS

Databases and Software

Axio Imager Software, Zeiss

Excel, Microsoft®

Image Lab, Bio-Rad

ImageJ, NIH

National Centre for Biotechnology Information, NCBI (https://ncbi.nlm.nih.gov)

Human Protein Atlas, HPA (https://www.proteinatlas.org/)

Ensembl (https://www.ensembl.org)

KEGG - Kyoto Encyclopedia of Genes and Genomes (https://www.genome.jp/kegg/)

GraphPad, Prism6

Zen Software, Blue Edition, Zeiss

LAS X, Leica

BD Accuri™ C6 Software, BD Biosciences

Annex 2

NAD metabolism in proteostasis poster exhibited in IV Postgrad Symposium in Biomedicine, 5 July 2018, Aveiro, Portugal

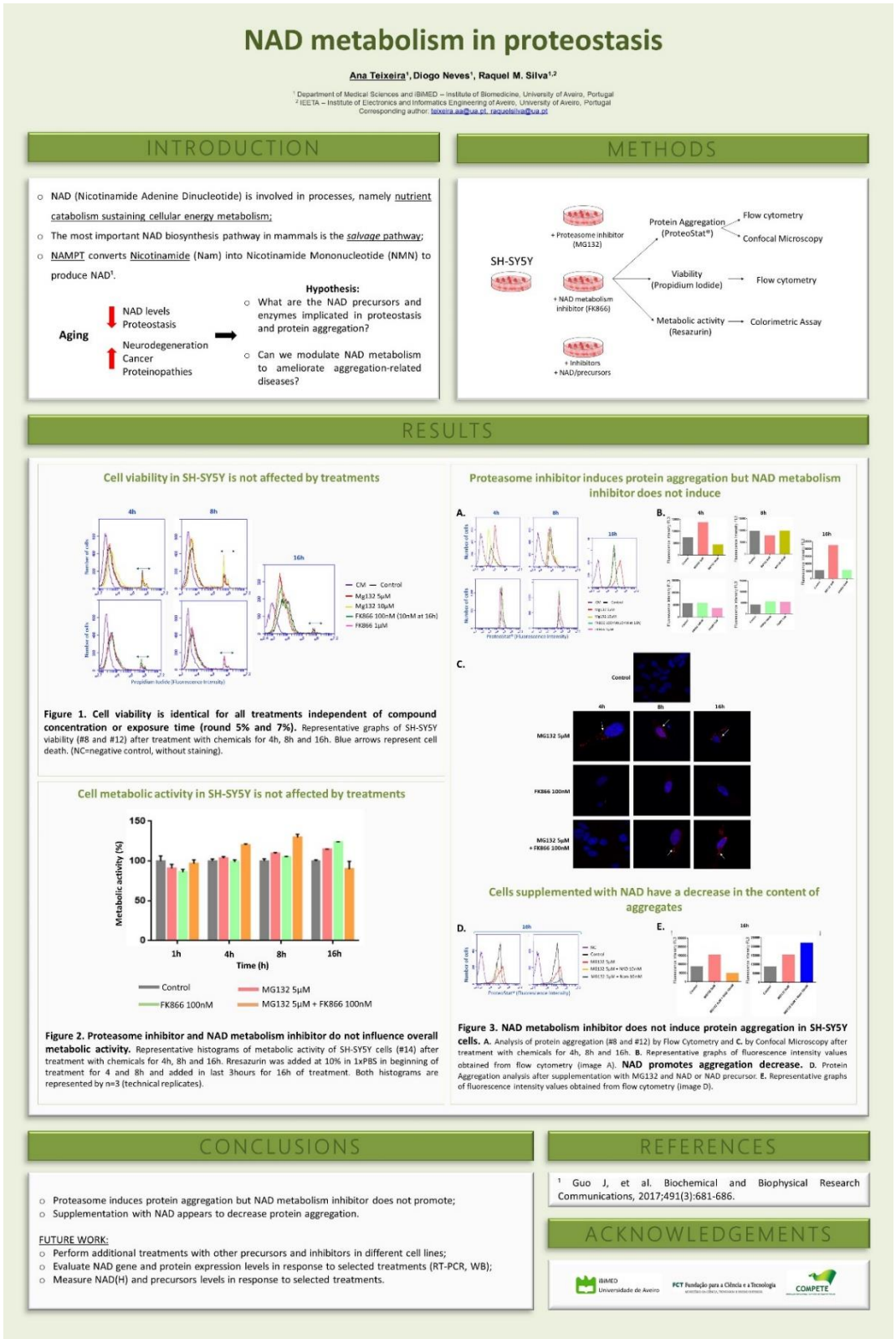

Annex 3

Evolutionary insights from the comparative analysis of hominid genomes poster exhibited in RECPAD 2018 – 24th Portuguese Conference on Pattern Recognition, 26 October 2018, Coimbra, Portugal

Evolutionary insights from the comparative analysis of hominid genomes

Ana Teixeira[1], Diogo Pratas[2], Armando J Pinho[2,3], Raquel M Silva[1,2]

[1]Department of Medical Sciences and iBiMED - Institute for Biomedicine, University of Aveiro [2]IEETA - Institute of Electronics and Informatics Engineering of Aveiro, [3]DETI - Department of Electronics, Telecommunications and Informatics

Introduction

- During the Late Pleistocene period (381,000-473,000 years ago), Neanderthals and Denisovans inhabited Eurasia while modern humans spread out of Africa around 350,000-35,000 years ago (1);
- Traces of Neanderthal genome were found among all non-African populations, suggesting that the admixture occurred when modern humans arrived to Eurasia (2,3);
- Nuclear DNA of Denisovan DNA appears to have higher diversity than Neanderthal DNA, but lower than modern humans and this group contributed to the genomes of present-day Australian Aborigines and American populations (4);
- Recently, a bone fragment was found from an individual with a Neanderthal mother and a Denisovan father, suggesting that the migrations of Neanderthals occurred before the spread of out-of-Africa by modern humans (5).

Fossils from ancient hominids showed differences in diversity and population dynamics. Therefore, our objective is to find and identify exact regions in the modern human genome (*Homo sapiens*) that could elucidate past events. Their discovery is important to identify evolutionary traits that could be related to novel functions or related to diseases. For that, we use a probabilistic method (CHESTER) to map and visualize those regions. This is a probabilistic method that is alignment-free with respect to the ancient genome.

Methods

CHESTER detect and visualise human specific regions based on the detection of relative absent words (RAWs) (6). The tool is divided into three programs: CHESTER-map for mapping the regions, CHESTER-filter for filtering and segmenting the regions and CHESTER-visual for visualizing the regions (7, 8).

The parameters used in this work are described next.

- CHESTER-map: Neanderthal (9) and Denisovan (10) genomes (reference) were used simultaneously against modern human DNA (target, GRCH38p7), using a Bloom filter with a size of 64 GB (m = 858,993,459,200), a k-mer model with high depth (k = 30) and with the "-i" parameter (handle inversions) for the mapping. Reads from reference genomes were used in FASTQ format while reads from target genome were used in FASTA format.
- CHESTER-filter: obtained coordinates from CHESTER-map were used to filter and segment the exact regions with a window size of 401 and 501bp (base pairs), a threshold value of 0.45 and 0.48 (-t) and a subsampling size of 1bp (-u).
- CHESTER-visual: exact regions were visualized with an enlarge (-e) of 500,000bp, chromosome by chromosome.

After setting the parameters, the tool works with the following algorithm:

- For each ancient DNA sequence:
- Given m, calculate the number of optimal hash functions (h);
- Calculate the probability p and the round value of h;
- Using a window size, the model updates each possible k-mer in the Bloom filter;
- Freeze the model (stop updating);

- For each human chromosomal sequence, search for each k-mer and for the inverted complemented k-mer, storing the result in a Boolean file:

- Store the individual results in a global Boolean file;
- Filter the global file, given a certain window size;
- Segment the filtered results, according to a threshold t, and store them in a file with their relative genomic coordinates (individual files);

- Finally, read the coordinates of the regions from each file and paint these in an image.

Results

For a window size of 401 and a threshold of 0,45 and 0,48, respectively, we found 150 and 195 exact regions (Figure 1A and 1B, respectively). For the same threshold values but a window size of 501, we found 100 and 172 regions, respectively (Figure 1C and 1D).
Having the genomic coordinates of the exact regions, we use them to find the corresponding sequence on modern human DNA. We found protein-coding genes, RNA genes and uncharacterized sequences.

Among protein-coding genes, we have found: COL24A1 (collagen type XXIV alpha 1 chain), GHR (growth hormone receptor), CLIC2 (chloride intracellular channel 2) and OR8G5 (olfactory receptor family 8 subfamily G member 5). These genes are involved in several biological processes, such as signal transduction, hematopoietic cell differentiation, hormone response, endocytosis, sense of smell, metabolism and ion transport.
In future work we will look for the genomic alterations between these regions (exact regions vs primitive hominid genomes) to identify its impact in evolution. We will also perform a gene ontology analysis to understand the role of these regions in cell biology and human health.

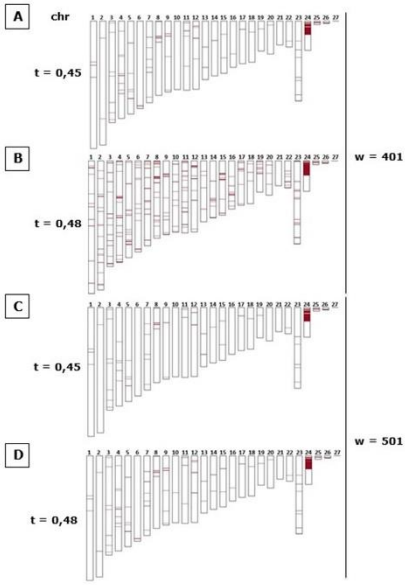

Figure 1: Representation of human specific region maps relative to Neanderthal and Denisovan genomes, by chromosome. Results were obtained using CHESTER with w = 401 and w = 501 with t = 0.45 and 0,48, and k = 30. Red strips represent exact regions.

Conclusions

RAWs are small exact regions present in a genomic sequence and their discovery and identification are important to understand evolution. In this study we used CHESTER to find these RAWs in modern human DNA. We found several regions that correspond to around 30 protein-coding genes that are involved in several cell functions. In the future, these regions may be studied to find the exact genomic alterations and its meaning in human evolution.

Acknowledgments

This work was partially funded by FEDER (Programa Operacional Factores de CompetitividadeCOMPETE) and by National Funds through the FCT-Foundation for Science and Technology, in the context of the projects UID/CEC/00127/2013, UID/BIM/04501/2013, POCI-01-0145-FEDER-007628, PTCD/EEI-SII/6608/2014, and the grant SFRH/BPD/111148/2015 to RMS.